9-1-2015

Development of Soft-Matter Delivery Systems: Coupling pH Responsive Polymers to Porous Silica Particles

Andrew Gomez

Andrew Gomez
Candidate

Biomedical Engineering
Department

This thesis is approved, and it is acceptable in quality and form for publication:

Approved by the Thesis Committee:

C. Jeffrey Brinker, Chairperson

Eric C. Carnes

Carlee E. Ashley

DEVELOPMENT OF SOFT-MATTER DELIVERY SYSTEMS: COUPLING PH RESPONSIVE POLYMERS TO POROUS SILICA PARTICLES

BY

ANDREW GOMEZ

B.S., Chemical Engineering, University of New Mexico, 2012

THESIS

Submitted in Partial Fulfillment of the
Requirements for the Degree of

Master of Science

Biomedical Engineering

The University of New Mexico
Albuquerque, New Mexico

July, 2015

DEDICATION

This work is dedicated to my wife. The strongest and bravest person I know who gave me the strength to complete this work. Jamie, thank you so much. You are the light of my life and my home.

ACKOWLEDGEMENTS

Throughout my thesis there are many people that deserve recognition and thanks for all their assistance and guidance. At the Center for Integrated Nanotechnologies, I thank Dr. George Bachand and Dr. Walter Paxton for user space in their labs and for all their guidance. I thank Dr. Katie Jungjohann for access to the TEM facility. I would like to thank Dr. Aaron Collins, a world class scientist, for all his help and input. His advice and expertise in optical measurements was invaluable and his "shop talk" lead to an increased understanding of polymer mechanics and polymer-particle interactions. Two people that were fundamental to my work were Dr. Ian Henderson and Dr. Adrienne Greene. Dr. Henderson was instrumental in all the polymer work, both in experiment and theory, and it has been an honor and a privilege to work with chemist of his high caliber. Dr. Greene, a brilliant nanoparticle biologist, aided with her extensive knowledge that traverses many academic fields and enabled significant growth of my work through her collaborative efforts. I thank my UNM advisor, Dr. C. Jeffrey Brinker, for all his help and my mentors Dr. Eric C. Carnes and Dr. Carlee Ashley. This has been a unique and great opportunity. I thank Patrick Fleig for all his knowledge and skills in particle production and the rest of the Carnes-Ashley lab. I thank my current employer Senior Scientific for their patience and understanding in finishing this work. And lastly, I thank my wife for all the support to get through this. Without these wonderful, talented people, none of this work would have been possible.

DEVELOPMENT OF SOFT-MATTER DELIVERY SYSTEMS: COUPLING PH RESPONSIVE POLYMERS TO POROUS SILICA PARTICLES

BY

ANDREW GOMEZ

B.S., Chemical Engineering, University of New Mexico, 2012

ABSTRACT

This work investigates polymeric coating of evaporated induced self-assembly (EISA) mesoprous silica nanoparticles for potential use in controlled drug release and therapeutics. As demonstrated here, lipid bilayer coatings can be easily replaced with different polymer analogs allowing for dynamic response to environmental stimuli. In addition to coupling commercially available diblock polymers we synthesized and characterized a unique dual hydrophilic pH responsive diblock copolymer, PEO-PAA. This hybrid polymeric-nanoparticle system drastically improves targeting and release capabilities through the modular ability to couple multiple different polymers. Furthermore, this work is supported by an improved method to form and study giant polymer vesicles (pGVs)

TABLE OF CONTENTS

TABLE OF CONTENTS (concluded)

CHAPTER 1

"Leviathan" polymersomes formed via simple gel-assisted rehydration

Adrienne C. Greene,[1] Ian M. Henderson,[1] Andrew Gomez,[2] Walter F. Paxton,[1] Virginia VanDelinder,[1] George D. Bachand[1]

[1]Center for Integrated Nanotechnologies, Sandia National Laboratories, Albuquerque, NM 87185, United States
[2]Center for Materials Science & Engineering, Sandia National Laboratories, Albuquerque, NM, 87185, United States

DISCLAIMER FOR SCIENTIFIC WORK CONTAINED WITHIN THIS CHAPTER

The following chapter, ""Leviathan" polymersomes formed via simple gel-assisted rehydration" represents collaborative work in which I contributed as an integral member in both experimentation and manuscript preparation. Neither I, nor any member of my committee, in no way claim ownership on the scientific study contained within this chapter. It is agreed upon that full intellectual ownership of the work detailed in this chapter belongs to the corresponding author Dr. George Bachand and 1st author Dr. Adrienne Greene of Sandia National Laboratories. Upon reviewing this material and signing (pass or fail), I, the members of this committee, and employees of these committee members contractually agree that they will not replicate these efforts or modify the work outlined here to produce a similar publication, nor file for a patent related to this work. Furthermore, the information contained in this chapter cannot be claimed solely for myself nor can any portion of it be claimed by any member of the thesis committee. Author contributions are listed at the end of the chapter.

Preface

Formation of polymer giant vesicles (pGVs) is important to the work of creating a soft-matter polymer-particle delivery system because it provides the unique opportunity to study polymer vesicles properties without being adjoined to a particle system. Polymer mechanics such as fluidity, elasticity, and response to environmental perturbation can easily be studied using this method. Originally, forming pGVs was attempted using a common method of platinum wire electroformation[1]. This yielded poor vesicle formation as seen in Figure 1 and only selectively worked with the different diblock copolymers. The gel rehydration is a universal method that forms pGVs with virtually any vesicle forming diblock copolymer in various rehydration solvents. Preliminary work showed efficient polymersome encapsulation of silica particles as discussed in Chapter 3. Similar to previous work of the protocell system[2], supported-lipid bilayers on mesoporous silica particles, liposomes were characterized and contrasted to the protocell system. In the same effort, gel rehydration is utilized to characterized polymersomes.

References

[1] B. M. Discher, Y. Y. Won, D. S. Ege, J. C. Lee, F. S. Bates, D. E. Discher, D. a Hammer, *Science* **1999**, *284*, 1143–1146.

[2] C. E. Ashley, E. C. Carnes, G. K. Phillips, D. Padilla, P. N. Durfee, P. a Brown, T. N. Hanna, J. Liu, B. Phillips, M. B. Carter, et al., *Nat. Mater.* **2011**, *10*, 389–397.

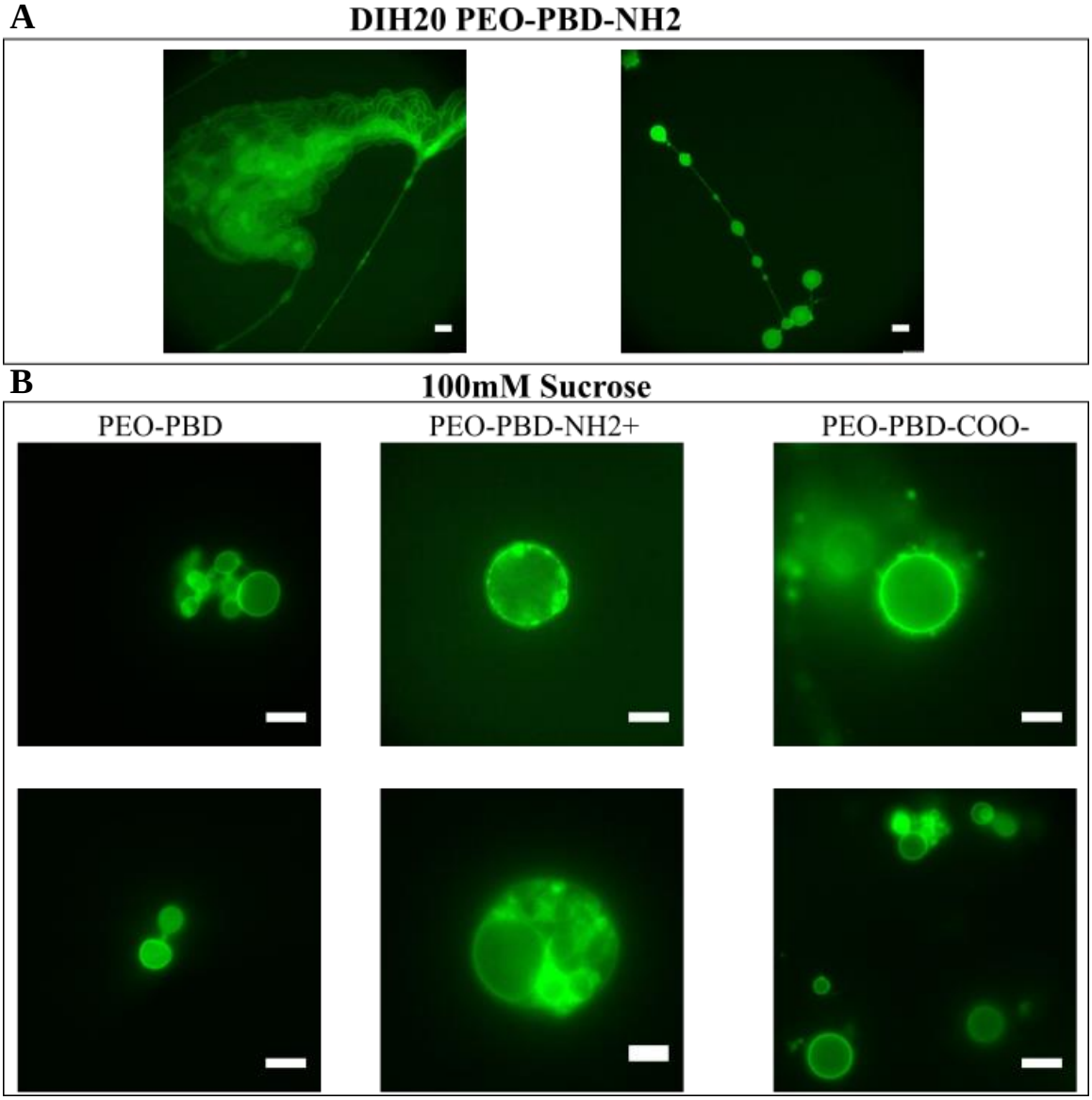

Figure 1. Poly(ethylene oxide)-b-poly(butadiene) (PEO-PBD, P2904, Polymer Source), amine and carboxylic acid functionalization, PEO-PBD-$NH2^+$ and PEO-PBD-COO^- giant vesicle electroformation using platinum wires. ~30uL of 5mg/ml polymers chloroform solution was deposited on 2 platinum wires spaced 1mm apart. Wire apparatus was placed under vacuum overnight. The wires were then placed in a 1.5mL cuvette of 100mM sucrose solution. Electroformation was conducted using an attack phase of 15min at 10hz and 0-2V, an envelope phase of 90 min at 10 hz and 2V, and a decay phase of 15-20 min at 4hz and 4V. The two images in top panel A represents formation of PEO-PBD-$NH2^+$ in DIH20. The bottom 6 images in panel B are formation of PEO-PBD, PEO-PBD-$NH2^+$ and PEO-PBD-COO^- in 100mM sucrose. Malformed self-assemblies were typically observed. Yield was poor of any spherical vesicles that did form which generally had polymer processes protruding from the vesicle surface or were asymmetric. Reproducibility using the same diblock polymers was problematic in addition to getting any vesicle formation using alternative diblock copolymers .

Abstract

Polymersomes are being widely explored as synthetic analogs of lipid vesicles based on their stability and enhanced properties. Here, we present for the first time, the rapid and high-yielding formation of giant (>4 μm) polymer vesicles (pGVs) using gel-assisted rehydration, and provide a mechanism of how formation and size distribution of pGVs may be achieved. Using this method, pGVs were formed from an array of polymer compositions and rehydration solutions, including cell culture media, rendering the technique broadly applicable for targeted and controlled release of therapeutic agents. pGV size was tunable by altering temperature during rehydration or adding fluidizers to the polymer membrane, generating "leviathan"-sized pGVs (>100 μm). The correlation between size and membrane fluidization suggests a unique mechanism from that proposed for lipid GUV formation in which both polymer diffusivity and osmotic potential drive the formation and size distribution of the pGVs.

Introduction

Giant vesicles (GVs) are biological membrane models created through the self-assembly of amphiphilic molecules[1]. While lipid GVs are excellent mimics of bio-membrane systems, they have inherent limitations, including short shelf life and degradation from various environmental perturbations. To overcome these restrictions, the use of polymersomes is being widely explored as synthetic analogs of lipid vesicles. Polymersomes are created through the self-assembly of amphiphilic block copolymers[2,3], and are renowned for their stability[4], robustness[5], chemical versatility[6,7], barrier properties[5,8], and tunable physical attributes[9–11]. Engineering versatile polymer combinations with additional alterations through surface modification,

changes of pH[12], and/or heat[12] allows polymersomes to be used in a wider range of applications over liposome analogs.

As polymersomes continue to both supplement and supplant lipid vesicles in many applications, the production and characterization of cell-sized, giant (>4 μm) vesicles becomes increasingly important[13]. These polymer giant vesicles (pGVs) are important for, among other things, characterizing the properties of the polymer bilayer[4,14], forming and studying polymer nanotubes by manipulation of the polymer bilayer[15,16], and investigating protein stabilization[17]. In addition to understanding these valuable physical characteristics, giant-sized polymersomes are essential candidates for use in developing long term synthetic biomimetic systems[16] and for controlled biological drug targeting and release[18–20]. Unfortunately, the actual production of pGVs is currently limited to a few labor-intensive and/or low-yield techniques such as electroformation[14], and templated rehydration[21].

Results and Discussion

Recently, a new technique has been developed to create lipid GUVs via gel-assisted rehydration[22]. This method involves depositing an organic solution of lipids onto a dehydrated gel, which, when rehydrated, forms lamellar structures that eventually coalesce into giant liposomes. Aside from being very convenient and simple, gel-assisted rehydration also enables GUVs to be created in physiological salt conditions, an important distinction from other techniques[22,23] and allows for easy reconstitution of membrane proteins in lipid vesicles[24].

Herein we investigated the use of gel-assisted rehydration as a method to form pGVs from amphiphilic block copolymers. A 1% (w/w) agarose solution was dissolved in water

and then a thin film of the agarose solution was deposited onto a glass coverslip and fully dehydrated (Scheme 1). Polymers dissolved in chloroform and mixed with a small percentage of fluorescently labeled lipid for visualization purposes were spread evenly across the dehydrated agarose film and excess chloroform was evaporated under a vacuum. The polymer film was then rehydrated with water on a hot plate at 40˚C for 1 hour unless otherwise noted (see Supporting Information for method details). Large populations of giant polymer vesicles with an average diameter of 5.8 μm ± 2.5 (mean ± standard error) did, in fact, form (Figure 1), with each sample consistently producing a several hundred intact pGVs. Timelapse photomicrographs show that pGV formation begins as early as 25 minutes post rehydration, starkly contrasting the lengthy methods of electroformation and templated rehydration (i.e. several hours) (Figure S1).

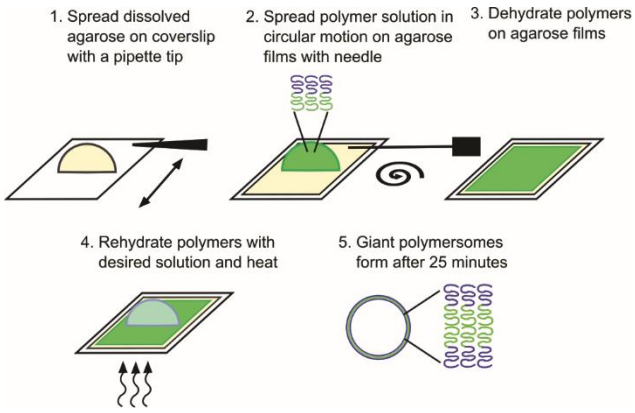

Scheme 1. Schematic depicting the gel-rehydration method to form giant polymersomes.

Traditional methods of pGV formation are typically limited to rehydration in sucrose solutions[14]. Using gel-assisted rehydration, poly(ethylene oxide)-*b*-poly(butadiene) (PEO-PBD, EO_{22}-BD_{37}) polymersomes were successfully formed in a variety of buffer solutions, including a full mammalian cell culture medium (Figure 1a). Likewise, a variety of different polymer compositions including different diblock copolymers such as

poly(ethylene oxide)-*b*-poly(ethylethylene) (PEO-PEE, EO_{22}-EE_{37}) successfully formed pGVs. A commercially available triblock co-polymer, poly(ethylene oxide)-*b*-poly(propylene oxide)-*b*-poly(ethylene oxide) (PEO-PPO-PEO, EO_{80}-PO_{27}-EO_{80}), partially formed pGV-like structures (Figure 1b and Table S1). Positively and negatively charged PEO-PBD polymers, synthetic analogs to naturally-occurring charged lipids, also robustly formed pGVs (Figure 1b). These data demonstrate that gel-assisted rehydration is a simple, fast and versatile method for forming a wide array of pGVs.

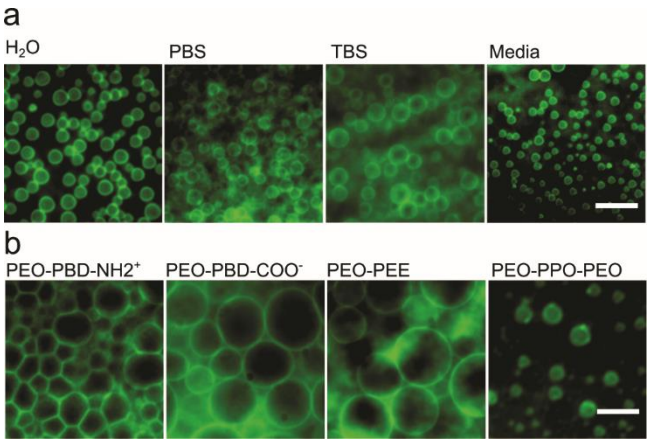

Figure 1. Polymersomes were formed in different buffers and from a variety of polymers (all at 40˚C for 1 hour on an agarose gel). (a) Epifluorescence images of PEO-PBD polymersomes made with different rehydration solutions. (b) Epifluorescence images of *p*GVs made with different polymer compositions in H_2O. Scale bars = 10 µm.

Different gel substrates were also tested for the formation of PEO-PBD pGVs including low melting point agarose, acrylamide and plain glass substrates. None of these substrates robustly produced pGVs (Figure S2), in contrast to lipid GUVs that form on a variety of different gel substrates[22]. Small polymersomes did form on the glass surface; the number of vesicles, however, was much lower than on the agarose films and the size was much smaller (<2 µm). pGVs formed preferentially on defects scratched into the agarose film prior to deposition of polymers as shown in Figure S3. These defects likely provide more surface area for the polymer to collect, increasing the reservoir of polymer

available for vesicle formation and/or more surface area for rehydration, thus increasing the efficiency of formation.

The fluidity of pGVs was characterized using fluorescence recovery after photobleaching (FRAP); representative photomicrographs of FRAP on a PEO-PBD polymersome are shown in Figure 2a. A small region of a pGV containing a small percentage of Liss-rhodamine-labeled lipid was bleached with a laser and the fluorescence recovery was monitored over several minutes. Fluorescence recovered after ~5 minutes, indicating that the polymer membrane is fluid. The fluorescence intensity recovery profiles for different polymer compositions are shown in Figure 2b. All of the polymersomes tested were fluid across expected timescales, and indeed were similar in recovery rate. This result is surprising given the much lower T_g of the PEE block in PEO-PEE as compared to PBD, indicating a possible fluidizing inclusion of free agarose from the gel. Diffusion coefficients were calculated (see SI for details) and compared across the different polymer membranes and values fell within expected ranges[15,25] (Table 1 and Figure S4).

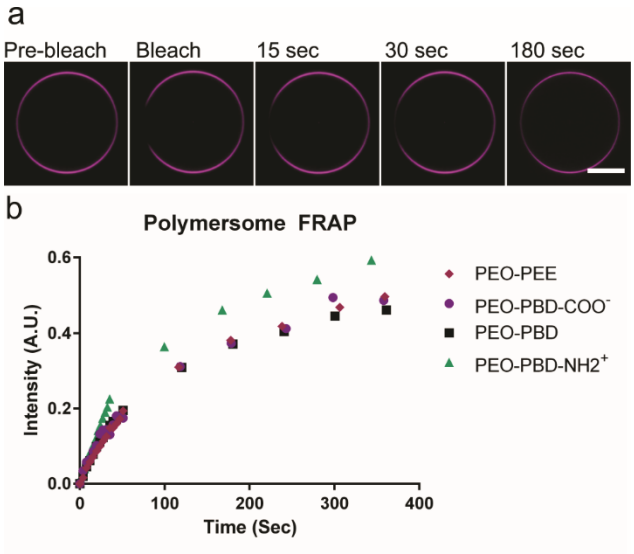

Figure 2. Fluorescence recovery after photobleaching (FRAP) analysis shows that polymersomes are fluid. (a) Epifluorescence imaging of a representative PEO-PBD *p*GV pre-, during and post-fluorescence bleaching. Scale bar = 10 µm. (b) Time-dependent fluorescence recovery profiles for different polymers.

Table 1. Diffusion coefficients (mean ± standard error) of different *p*GVs.

Polymer	**Diffusion (µm^2/sec)**
PEO-PBD	0.0144 ± 0.006
PEO-PBD-COO$^-$	0.0244 ± 0.003
PEO-PBD-NH2$^+$	0.0142 ± 0.007
PEO-PEE	0.0287 ± 0.009

Size control of the pGVs was easily attained by altering the temperature during rehydration. As the temperature increased, the average size of the polymersomes increased (Figure 3). ANOVA analysis of the average diameter of the polymersomes confirmed that temperature significantly effects pGV size ($P < 0.001$; Table S2). Furthermore, pairwise comparisons of these data reveal significant differences in pGV size among all of the samples ($P < 0.03$) except between the 60°C and 70°C samples in which the average sizes were not significantly different ($P = 0.069$). Frequency distributions for the polymersome populations revealed an increase in the dispersity of

the distribution and standard deviation as the temperature was increased (Figure 3c). The use of temperature provides a predictable, simple and more rapid approach to control pGV size compared to other techniques[21,26].

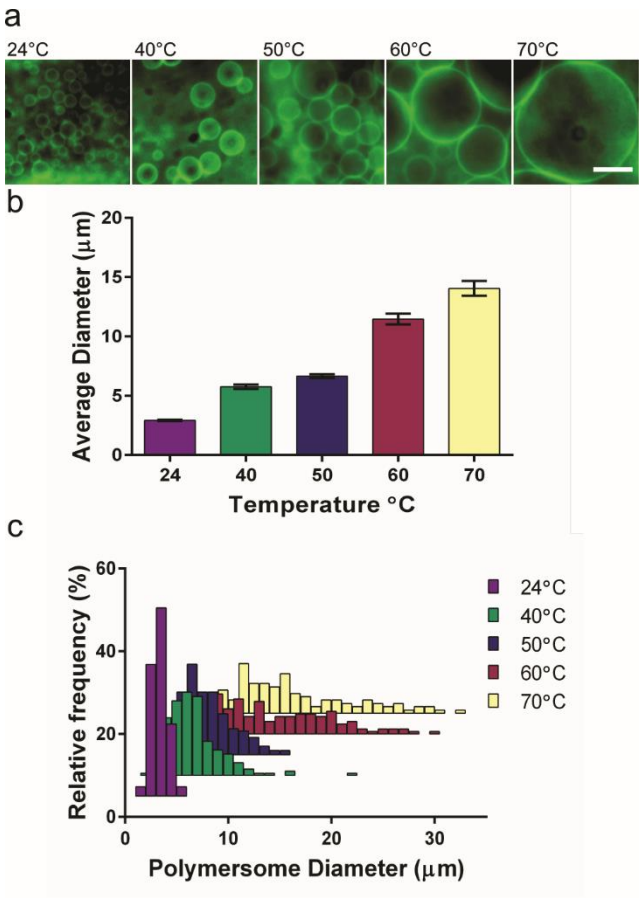

Figure 3. Polymersome GU\V size is tuned using different rehydration temperatures. PEO-PBD polymersomes were generated in water on 1% agarose gels for 30 minutes at varying temperatures on a hot plate. (a) Epifluorescence images of polymersomes made at increasing temperatures. Scale bar is 10 μm. (b) Average diameters of polymersomes made at different temperatures. Error bars are standard error of the mean. (c) Percent frequency distribution of polymersomes made at varying temperatures (>100 polymersomes analyzed per condition).

Previous reports using gel-assisted rehydration to form lipid vesicles suggest that the mechanism of formation consists of liposome swelling upon rehydrating followed by vesicle fusion due to mechanical crowding, creating large GVs[27]. Polymersomes, however, require specific conditions (e.g. addition of salts and agitation[11]) to facilitate vesicle fusion, so the mechanism of pGV formation using gel-rehydration likely is quite

different from the formation of liposomes. Other reports suggest that increasing the osmotic pressure during liposome formation (e.g. by adding sucrose to the gel) helps in the formation and detachment of vesicles from the surface[28,29]. To explore the role of osmotic potential in pGV formation, we prepared dehydrated agarose gels that incorporated small ionic or neutral molecules. Agarose was dissolved either in phosphate buffered saline (PBS) solutions or in sucrose solutions. Polymer films were then formed on the different agarose gel conditions. Rehydration of films on these gels was expected to result in vesicles with an internal solution of higher osmolarity than the external rehydration solution. Interestingly, vesicles did not form on gels prepared in PBS and rehydrated with water, while gels prepared in water and rehydrated with PBS did form pGVs (Figure 1b). We attribute the unexpected lack of vesicle formation on PBS gels to the failure of the agarose gel to rehydrate, thereby preventing polymer film rehydration. Restricted gel rehydration is likely driven by the strong ionic effects from the PBS buffer, which may precipitate the agarose polymer and prevent rehydration.

In contrast, the addition of sucrose resulted in increased vesicle size when (*i*) the gel was prepared in a sucrose solution, (*ii*) sucrose was in the rehydration solution and (*iii*) sucrose was used in both the agarose gel preparation and in the rehydration solution (Figure 4a and b). Two-way ANOVA analysis of vesicle size with the different conditions confirmed that there is an interactive effect of gel type and rehydration solution on diameter ($P < 0.001$). All parameters were significantly different from the other conditions ($P < 0.001$) except for rehydration with water on a gel made with water and rehydration with water on a gel made with sucrose, which did not differ significantly ($P = 0.15$).

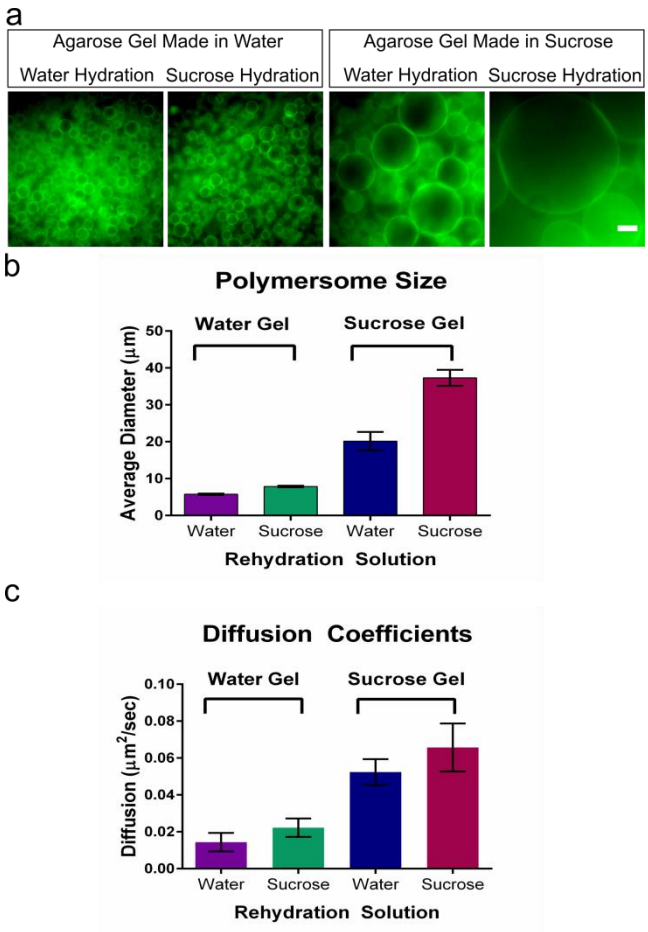

Figure 4. Addition of sucrose during rehydration results in larger polymersome GVs. (a) Epifluorescence images of GUVs formed on either 1% agarose gels in water (first two images) or 1% agarose gels in 100 mM sucrose (last two images) and rehydrated in either water or 100mM sucrose as indicated at the top of the image. Scale bar = 10 μm. (b) Average diameter of GUVs formed in the indicated conditions. Error bars are standard error of the mean. (c) Diffusion coefficients (mean ± standard deviation) of the different polymersomes.

Balancing the equilibrium of the system by hydrating a gel made with sucrose using a sucrose solution resulted in the most rapid formation of pGVs (~5 minutes), the largest diameter, and the broadest size distribution. Here, populations of "leviathan"-sized polymer vesicles measuring 100 μm or greater in diameter were formed (Figure S5). Sucrose addition in the rehydration solution and in the gel, respectively, increased the diffusion of the polymer membrane, indicating that sucrose is fluidizing the membrane and aiding in the formation of pGVs (Figure 4c). Addition of sucrose at the different steps resulted in a steady increase in the diffusion coefficient, with the highest diffusion

occurring when the gel was made in sucrose and the polymers were also rehydrated with sucrose (Figure 4c). Thus, in addition to osmotic effects described above, sucrose has a strong fluidizing effect on the membrane that can also enhance the size of vesicles. This differs from the proposed role of sucrose in the formation of lipid GUVs, which is thought to be predominately osmotic[28,29]. However, previous work has shown that increasing the temperature in a lipid bilayer or adding carbohydrates to a lipid monolayer both result in the expansion of the average lipid molecule surface area and likely cause a membrane fluidizing effect[30,31]. Other work has shown that the formation of bilayer membranes on polysaccharide-coated surfaces increases the fluidity of the membrane[32]. Interestingly, sucrose has been added to live cell membranes to increase the fidelity of freeze-drying and been shown to increase live cell membrane fluidity[33]. Together, these results are in agreement with our data in which pGV size is increased by increasing the temperature or adding sucrose to the gel, resulting in a combination of fluidizing and osmotic effects.

Fluidizing the membrane with the addition of sucrose resulted in successful formation of pGVs with high molecular weight polymers. Attempts to form pGVs from these polymers using water resulted in poorly formed vesicles, however, the addition of sucrose aided in pGVs formation from these polymers: EO_{34}-BD_{46}, EO_{52}-BD_{93}, and EO_{89}-BD_{120} (Figure S6). In all cases, vesicle diameter was limited to around 1-5 μm, and vesicle formation occurred almost exclusively in defects. These results further support a combinatorial effect of an osmotic gradient and membrane fluidization in the formation of giant vesicles.

In summary, we have shown that gel-assisted rehydration is a convenient method for producing giant, cell-sized polymer pGVs. In addition to the broad applicability of this technique, tuning vesicle size may be achieved using temperature, osmotic gradients and small-molecule fluidizers. We propose a mechanistic model of formation in which membrane fluidization and osmotic pressure aids in pGV formation. With the aid of fluidizers, vesicles size may be increased to upwards of 100 μm. This technique is capable of reliably producing pGVs from different polymer compositions and charges with far better yields and much less difficulty than traditional methods. Furthermore, vesicles formed in biological buffers and media make them readily useful for biomimicry studies. The ability to consistently produce giant vesicles with different polymers and rehydration media, and with the capability to tune size, makes this a tailorable and versatile technique for many applications.

Author Contributions

Adrienne C. Greene (imaging, polymersome preparation, data analysis, manuscript preparation and intellectual contributions), Ian M. Henderson (polymer synthesis and characterization, gel preparation, manuscript preparation and intellectual contributions), Andrew Gomez (surface functionalization, electroformation, FRAP acquisition/analysis, manuscript preparation and intellectual contributions), Virginia Vandelinder (initial experimental design), Walter F. Paxton (intellectual contributions), George D. Bachand (data analysis and intellectual contributions).

Acknowledgements

This work was supported by the U.S. Department of Energy, Office of Basic Energy Sciences, Division of Materials Sciences and Engineering (BES-MSE). A.C. Greene, A. Gomez, W.F. Paxton and G.D. Bachand were supported by BES-MSE. I.M. Henderson and Virginia Vandelinder were supported through the Center for Integrated Nanotechnologies. This work was performed, in part, at the Center for Integrated Nanotechnologies, an Office of Science User Facility operated for the U.S. Department of Energy (DOE) Office of Science (user project number RA2015A0004). Sandia National Laboratories is a multi-program laboratory managed and operated by Sandia Corporation, a wholly owned subsidiary of Lockheed Martin Corporation, for the U.S. Department of Energy's National Nuclear Security Administration under contract DE-AC04-94AL85000.

References

[1] O. Wesolowska, K. Michalak, J. Maniewska, A. B. Hendrich, *Acta Biochim. Pol.* **2009**, *56*, 33–39.

[2] D. E. Discher, A. Eisenberg, *Science* **2002**, *297*, 967–973.

[3] D. E. Discher, F. Ahmed, *Annu. Rev. Biomed. Eng.* **2006**, *8*, 323–341.

[4] H. Bermudez, A. K. Brannan, D. a. Hammer, F. S. Bates, D. E. Discher, *Macromolecules* **2002**, *35*, 8203–8208.

[5] B. M. Discher, Y.-Y. Won, D. S. Ege, J. C.-M. Lee, F. S. Bates, D. E. Discher, D. A. Hammer, *Science (80-.).* **1999**, *284*, 1143–1146.

[6] R. C. Amos, A. Nazemi, C. V. Bonduelle, E. R. Gillies, *Soft Matter* **2012**, *8*, 5947.

[7] S. Egli, M. G. Nussbaumer, V. Balasubramanian, M. Chami, N. Bruns, C. Palivan, W. Meier, *J. Am. Chem. Soc.* **2011**, *133*, 4476–4483.

[8] R. Rodríguez-García, M. Mell, I. López-Montero, J. Netzel, T. Hellweg, F. Monroy, *Soft Matter* **2011**, *7*, 1532.

[9] K. T. Kim, J. J. L. M. Cornelissen, R. J. M. Nolte, J. C. M. Van Hest, *Adv. Mater.* **2009**, *21*, 2787–2791.

[10] W. F. Paxton, D. Price, N. J. Richardson, *Soft Matter* **2013**, 11295–11302.

[11] I. M. Henderson, W. F. Paxton, *Angew. Chemie - Int. Ed.* **2014**, *53*, 3372–3376.

[12] D. Schmaljohann, *Adv. Drug Deliv. Rev.* **2006**, *58*, 1655–1670.

[13] P. Walde, K. Cosentino, H. Engel, P. Stano, *ChemBioChem* **2010**, *11*, 848–865.

[14] B. M. Discher, *Science (80-.).* **1999**, *284*, 1143–1146.

[15] J. C. M. Lee, M. Santore, F. S. Bates, D. E. Discher, *Macromolecules* **2002**, *35*, 323–326.

[16] W. Paxton, N. F. Bouxsein, I. Henderson, A. Gomez, G. Bachand, *Nanoscale* **2015**, DOI 10.1039/C5NR00826C.

[17] V. Pata, N. Dan, *Biophys. J.* **2003**, *85*, 2111–2118.

[18] S. Ganta, H. Devalapally, A. Shahiwala, M. Amiji, *J. Control. Release* **2008**, *126*, 187–204.

[19] G.-Y. Liu, C.-J. Chen, J. Ji, *Soft Matter* **2012**, *8*, 8811.

[20] K. Moodley, V. Pillay, Y. E. Choonara, L. C. du Toit, V. M. K. Ndesendo, P. Kumar, S. Cooppan, P. Bawa, *Int. J. Mol. Sci.* **2012**, *13*, 18–43.

[21] J. R. Howse, R. a L. Jones, G. Battaglia, R. E. Ducker, G. J. Leggett, A. J. Ryan, *Nat. Mater.* **2009**, *8*, 507–511.

[22] K. S. Horger, D. J. Estes, R. Capone, M. Mayer, **2009**, 2973–2982.

[23] F. C. Tsai, B. Stuhrmann, G. H. Koenderink, *Langmuir* **2011**, *27*, 10061–10071.

[24] J. S. Hansen, J. R. Thompson, C. Hélix-Nielsen, N. Malmstadt, *J. Am. Chem. Soc.* **2013**, *135*, 17294–17297.

[25] D. a Christian, A. Tian, W. G. Ellenbroek, I. Levental, K. Rajagopal, P. a Janmey, A. J. Liu, T. Baumgart, D. E. Discher, *Nat. Mater.* **2009**, *8*, 843–849.

[26] R. J. Hickey, J. Koski, X. Meng, R. a Riggleman, P. Zhang, S.-J. Park, *ACS Nano* **2014**, *8*, 495–502.

[27] K. S. Horger, D. J. Estes, R. Capone, M. Mayer, *J. Am. Chem. Soc.* **2009**, 2973–2982.

[28] A. Weinberger, F. C. Tsai, G. H. Koenderink, T. F. Schmidt, R. Itri, W. Meier, T. Schmatko, A. Schröder, C. Marques, *Biophys. J.* **2013**, *105*, 154–164.

[29] K. Tsumoto, H. Matsuo, M. Tomita, T. Yoshimura, *Colloids Surfaces B Biointerfaces* **2009**, *68*, 98–105.

[30] J. H. Crowe, M. A. Whittam, D. Chapman, L. M. Crowe, *Biochim. Biophys. Acta* **1984**, *769*, 151–159.

[31] J. Pan, S. Tristram-Nagle, N. Kucerka, J. F. Nagle, *Biophys. J.* **2008**, *94*, 117–24.

[32] M. Haratake, E. Takahira, S. Yoshida, S. Osei-Asante, T. Fuchigami, M. Nakayama, *Colloids Surfaces B Biointerfaces* **2013**, *107*, 90–96.

[33] H. Li, M. Lu, H. Guo, W. Li, H. Zhang, *J. Food Prot.* **2010**, *73*, 715–719.

Supporting Information

Polymer Preparation and Characterization

Preparation and characterization of mesyl-PEO-PBD

A 100 mL RBF was charged with 1.03 g PEO-PBD (P2904, Polymer Source, Inc.) and 30 mL of methylene chloride (dried over CaH_2) and fitted with a stirbar and septum. The polymer was dissolved and the solution sparged with dry nitrogen for 15 min after which the flask was cooled in an ice-bath and sparged with N_2 for a further 10 min. After this time, 0.5 mL of methanesulfonyl chloride was added via syringe through the septum, and the mixture was stirred with ice-bath cooling for 5 min. After this time, 0.85 mL TEA (dried over sodium sulfate) was added slowly to the flask via syringe through the septum. The mixture was allowed to come to room temperature while stirring under N_2, and was allowed to continue stirring under these conditions for a total of 15 h.

After stirring for 15 h the contents of the flask were diluted to 300 mL with methylene chloride, and washed with pH 2 (HCl) water (3 × 300 mL) and then washed with saturated sodium bicarbonate in water (3 × 300 mL). Finally, the organic fraction was dried over sodium sulfate and evaporated to dryness. 0.60 g recovered: 58% NMR (90 MHz $CDCl_3$): δ = 5.5-4.5(br, 108H, PBD alkenes), 4.28 (t, 2H, $-CH_2-C\underline{\boldsymbol{H_2}}-O-SO_2CH_3$) 3.6 (br, 86 H, PEO backbonde), 3.01 (s, 3H, $-O-SO_2C\underline{\boldsymbol{H}}_3$) 2.3-0.5 (br, 108H, PBD backbone).

Preparation and characterization of phthalimidyl-PEO-PBD

To a 50 mL RBF was added 0.45 g Mesyl-PEO-PBD, 0.30 g potassium phthlamide, and 10 mL DMF. The flask was fitted with a stirbar and septum, and was

sparged with N_2 while heating to 50 °C. After 30 min of sparging the reaction mixture was cooled to room temperature and stirred under N_2 overnight. The DMF was then removed *in vaccuo* and replaced with 15 mL of THF. The excess potassium phthalimide was removed via filtration, and the polymer was purified via preparatory GPC. 0.135 g recovered. NMR (90 MHz $CDCl_3$): δ = 7.71 (br, 4H, phthalyl group), 5.5-4.5 (br, 108H, PBD alkenes), 3.6 (br, 86 H, PEO backbonde), 2.3-0.5 (br, 108H, PBD backbone).

Preparation and characterization of amino-PEO-PBD

The phthalimidyl polymer (0.125 g) was placed in a 25 mL RBF with 10 mL of ethanol and a stir bar. Once the polymer was taken up into the ethanol (turgid solution), 0.5 mL of hydrazine hydrate was added. A reflux condenser was fitted to the flask, and the entire apparatus purged via vacuum/backfill with N_2. The solution was brought to reflux under N_2 for 1 h. At the end of this time, the ethanol was removed under vacuum and the polymer re-dissolved in THF and purified via preparatory GPC. The deprotection of the amine was denoted by the disappearance of the Phthalimide peaks in NMR. 42 mg recovered.

Preparation and characterization PEO-PBD ethyl ester

A 50 mL RBF was charged with 0.43 g of PEO-PBD and 20 mg of a 60% NaH dispersion in mineral oil. The flask was fitted with a septum and purged for 10 min with dry N_2. After this, 10 mL of anhydrous THF was added vial syringe through the septum, the resulting solution being sparged with N_2 for 20 min. The solution was allowed to stir another 20 min under N_2 before 0.1 mL of ethyl bromoacetate was added through the septum. After the addition, the resulting mixture was stirred under nitrogen for a further 3

h, as it turned from an opaque white suspension to an opaque brown suspension. After this time was up, the suspension was filtered through a 0.2 μm syringe filter before being purified by preparatory GPC. 0.32 g was recovered. NMR (90 MHz $CDCl_3$): δ = 5.5-4.5 (br, 108H, PBD alkenes), 4.1, (t, 2H, C(O)C***H***$_2CH_2$), 3.6 (br, 86 H, PEO backbonde), 2.87 2.3-0.5 (br, 108H, PBD backbone).

Preparation and characterization PEO-PBD-carboxyalte

In a 50 mL RBF, 44 mg of PEO-PBD Methyl ester was added dissolved in 1 mL of THF. To this was added 10 mL of 5 wt% KOH in water. The mixture was stirred over night at 50 °C under N_2. The mixture was then acidified with HCl until the pH was approximately 2. The organic phased was then extracted into 3 × 10 mL methylene chloride, and then purified by preparatory GPC.

Polymer	M_w(total)	Composition	Charge	*p*GUV Formation
PEO-PBD (P2904)	2950	EO_{22}-Bd_{37}	Neutral	Yes
PEO-PBD (P9757)	4000	EO_{34}-Bd_{46}	Neutral	Partial
PEO-PBD (P3403) [§]	7300	EO_{52}-Bd_{93}	Neutral	Partial
PEO-PBD (P4753)	10400	EO_{89}-Bd_{120}	Neutral	Very small
PEO-PBD-NH^{2+}	2950	EO_{22}-Bd_{37}	Positive	Yes
PEO-PBD-COO^-	2950	EO_{22}-Bd_{37}	Negative	Yes
PEO-PEE	3050	EO_{22}-EE_{37}	Neutral	Yes
PEO-PPO-PEO	8350	EO_{80}-PO_{27}-EO_{80}	Neutral	Partial
PS-PEO	5000	EO_{34}-PS_{34}	Neutral	No

[§] 1,4 addition.

Table S1. Summary of the characteristics of different polymers tested and their formation of *p*GUVs. Composition lists the chain length of the indicated polymer blocks. Partial formation indicates polymersomes did not fully detach from the surface and/or formed polymersome-like structures, but did not form a fully intact polymersome.

Formation of agarose films on glass slides by deposition

The original protocol detailing the formation of agarose films for liposome formation[1] was adapted to the formation of pGVs. We dissolved 1% (w/w) agarose (Sigma-Aldrich, St. Louis, MO) in deionized water by boiling and allowed agarose to

solidify. The agarose was then melted in the microwave and 300 µL of agarose solution was deposited onto a 25 mm square #1 glass coverslip (VWR, Radnor, PA). The long edge of another pipette tip was used to spread the agarose solution evenly on the coverslip surface. Agarose films were dehydrated by incubating at 40 °C for >1 hour and stored until use.

Formation of polymer films on the prepared agarose films

All polymers were prepared in chloroform at a 5 mg/mL concentration with 0.5 mol% of either Lissamine Rhodamine B PE lipid or 0.5 mol% NBD-PC lipid (Avanti Polar Lipids, Inc., Alabaster, AL) for epifluorescence imaging purposes. 30 µL polymer solutions were deposited onto the agarose films and spread evenly across the agarose using the long edge of a needle. Polymer films were placed under house vacuum overnight to fully remove any solvent residues.

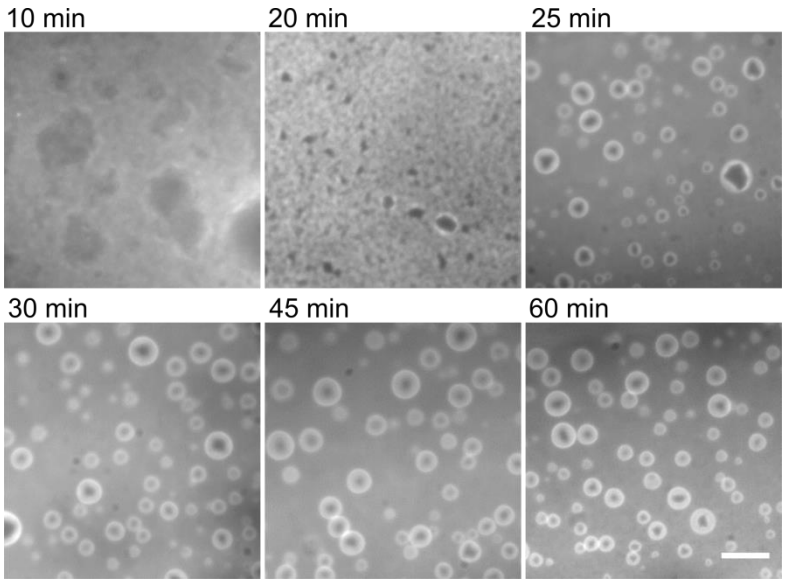

Figure S1. Time-lapse of polymersome GUV formation. Epifluorescence images depict PEO-PBD polymersome formation over the course of 1 h on an agarose gel at 40 °C. Scale bar is 10 µm.

Formation of polymersomes on different substrates and using different rehydration media

Several different gel substrates were made and tested for the formation of pGVs on the different surfaces. We made a 1% (w/w) ultra pure low melting point agarose gel (Life Technologies, Grand Island, NY) using the same method as for the regular agarose gels and also polyacrylamide gels (synthesis described below). We tested the following different agarose gel conditions: 1% (w/w) agarose dissolved in 1× phosphate buffered saline (137 mM NaCl, 2.7 mM KCl, 10 mM Na_2HPO_4, 1.8 mM KH_2PO_4, pH 7.4) and 1% (w/w) agarose dissolved in 100 mM sucrose in water. We formed PEO-PBD (P2904) neutral polymer films on the different gel substrates and different gel conditions as well as a plain glass substrate.

While the sucrose-saturated gels worked well for vesicle formation, the PBS buffer-saturated gels showed no indication of vesicle formation. Likewise, glass, low melt agarose gels, and polyacrylamide gels showed no appreciable vesicle formation (see Figure S2).

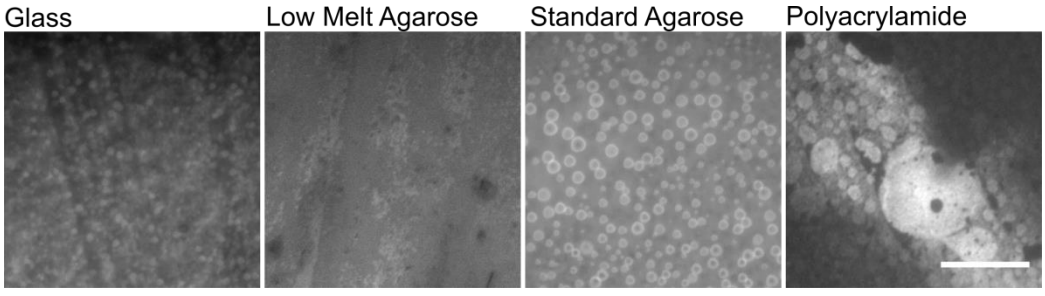

Figure S2. Polymersome GUVs form poorly on different substrates. Epifluorescence photomicrographs of PEO-PBD polymersome formation on the indicated substrates after 1 h at 40 °C. Scale bar is 10 μm.

Amide gel preparation

Cover slips (25 mm × 25 mm, VWR, Radnor, PA) were cleaned with piranha solution and rinsed with deionized water before use and dried in a 50 °C oven for 1 h before use. The slides were placed in a Teflon slide holder and lowered into a jar containing 200 mL of anhydrous toluene and 5 mL of (3-aminopropyl)triethoxysilane (APTES, Sigma-Aldrich, St. Louis, MO). The reaction vessel was heated to 50 °C under N_2 for 2 h. After this time, the slides were washed with acetone, and deionized water, then returned to the slide holder. After a final wash with MeOH, the slides were dried in a 50 °C oven for 30 min.

After drying, the slides were placed in an oven-dried 300 mL jar containing a stirbar, to which was cannulated 150 mL of anhydrous benzene. The jar was placed in an ice bath and allowed to cool for 20 min. Under a stream of N_2, 5 mL of methacyloyl chloride was added, and the mixture stirred under N_2 for 5 min. After this, 5 mL of tripropyl amine was added to the reaction mixture, the jar was capped and the solution allowed to warm to room temperature overnight.

The slides were removed from the jar an again washed with acetone, methanol, and water. To 10 mL of deionized water was added 0.95 g of acrylamide, and 0.056 g of methylene bis-acrylamide. Once this mixture had dissolved, 50 μL of a 10% (w/v) solution of ammonium persulfate was added, and the mixture agitated to insure homogeneity. After this, 10 μL of TEMED was added to the mixture, which was once again agitated. The solution was transferred to the slide via a syringe, with 1 mL of solution for each cover slip. The gel formed within 20 min, and each cover slip was placed in deionized water (10 mL) for at least 4 h before use.

Formation of polymer giant vesicles

Unless otherwise stated, all polymersomes were generated using the following method: PDMS wells were adhered to the agarose/polymer films and 500 µL deionized water was deposited into the well. Films were incubated for 60 min on a 40°C hotplate prior to imaging directly on the surface. For the buffer compatibility experiments, polymer films were rehydrated in 500 µL of 1x PBS (137 mM NaCl, 2.7 mM KCl, 10 mM Na_2HPO_4, 1.8 mM KH_2PO_4, pH 7.4), 1x tris buffered saline (50 mM Tris-Cl, pH 7.5, 150 mM NaCl), 100 mM sucrose in water, or full cell culture media (Dulbecco's Modified Eagle Medium [Life Technologies, Grand Island, NY], supplemented with 10% fetal bovine serum and 10mM L-glutamine).

The effect of temperature on the formation of pGVs was tested using the procedure stated above, but incubated on a hotplate with the following temperatures: 24˚C, 40˚C, 50˚C, 60˚C and 70˚C. Polymersome diameter size was measured using Fiji imaging software[2] (>100 polymersomes/condition) and size distributions were plotted using GraphPad Prism statistics software (La Jolla, CA) (see Table S2). ANOVA analysis was performed using SigmaPlot (San Jose, CA).

Temperature	Mean diameter (µm)	Min	Max	Range	Standard Deviation
24˚C	2.928	1.431	4.839	3.408	0.741
40 ˚C	5.760	1.446	20.571	19.125	2.532
50˚C	6.654	2.017	14.126	12.109	2.361
60˚C	11.463	2.284	25.420	25.420	5.826
70˚C	14.043	2.863	32.635	32.635	6.984

Table S2. Descriptive statistics from ANOVA analysis on the size distribution of PEO-PBD polymersomes made at different temperatures.

Preferential formation of pGVs **on defects**

In the course of our investigation, it was repeatedly observed that vesicles preferentially form on defects in the gel (Figure S3). Agarose gels were made as described and defects were scratched into the gel using a needle prior to depositing the polymer solution. Defects were also etched into polymer films already formed on the agarose gel surface. Preferential formation of polymersome GUVs occurred on defects etched in the agarose layer prior to the deposition of polymers. This is thought to be due to the defect serving as a point of egress for water, allowing for more rapid and complete rehydration of the polymer film.

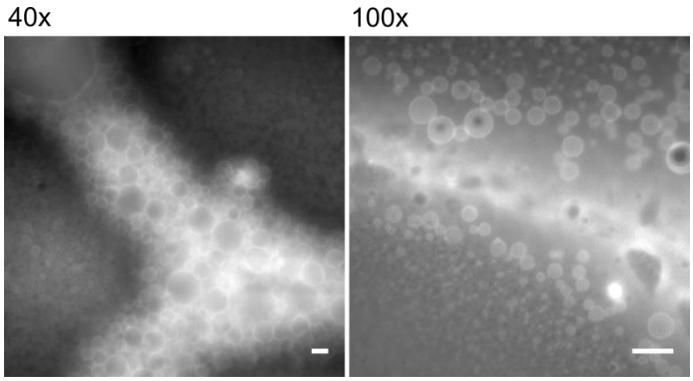

Figure S3. Polymersome GUVs form preferentially on gel defects. PEO-PBD polymersomes were generated in water at 40 °C on agarose gels that had been scratched to create defects. Epifluorescence images of polymersomes formed on gel defects at a 40× and 100× magnification. Scale bars are 10 μm.

Imaging the pGVs **on and off the surface of agarose films**

The polymersomes were imaged using an inverted microscope (Olympus IX81) in epifluorescence with either a 40× or 100× objective (as noted in the text). Images were captured using an Orca-Flash 4.0 cMOS camera (Hamamatsu Photonics, San Diego, CA) and processed using Fiji imaging software[2]. Polymersomes were imaged either directly on the agarose film surface or removed from the agarose surface and adhered to a clean

glass substrate. To remove the polymersomes, coverslips were allowed to incubate overnight at room temperature and gently pipetted off of the surface using a 200 µL pipette with the end of the tip cut off and gently repeated up and down pipetting. Surface modified coverslips were used to minimize floating and movement of detached polymersomes. Circular silicone isolator wells (Electron Microscopy Sciences, Hatfield, PA) of diameter 9 mm and depth 0.5 mm were added to modified coverslips. Polymersomes were added to the well enclosure area and sealed with another coverslip for incubation. Minimum incubation time was 15 min-1 h. For incubation longer than 1 h, coverslips were placed in a humidity chamber to prevent evaporation. Coverslips treated with ozone for 15 min were used to create hydrophilic surfaces and worked well for imaging neutral polymersomes. COO^- polymersomes were imaged on piranha cleaned coverslips treated with APTES. APTES functionalization was done following standard APTES-coating protocols. Briefly, 2% APTES, 5% deionized water, and 93% of 95% ethanol was mixed and hydrolyzed for 5 min before adding to the coverslips. Coverslips were functionalized with APTES for 10 min followed by 4-5 rinses with 95% ethanol. The coverslips were then cured for 15 min at ~100 ˚C. Polymersomes were added to gasket enclosure and incubated for imaging as previously described. $NH2^+$ polymersomes were difficult to recover from the agarose surface using pipette removal. Previous in house experiments studies, using $NH2^+$ polymersomes formed by electroformation methods showed that casein passivated glass assists in bringing $NH2^+$ polymersomes down to the surface, even though the production yield was low. Coverslips were treated with ~18 mg/mL of casein in tris buffer for 5 min. The casein solution was then wicked off followed by the additional of the $NH2^+$ polymersomes. Minimum incubation time was

2-4 h. Additionally, polymersomes formed in sucrose can also be diluted in a glucose solution of the same osmolarity to bring polymersomes down to the surface.

Fluorescent Recovery After Photobleaching (FRAP) analysis of polymersomes

To characterize fluidity of the polymersome membranes, FRAP imaging was performed on a FV-1000 Olympus IX-81Confocal Laser Scanning Microscope, with FV10-ASW software. A 60× oil objective or 40× air objective was used depending on polymersome size. A multi-line Argon laser was used for excitation at 488 nm and 543 nm for NBD and Lissamine Rhodamine dyes respectively. Fluorescence data processing was done using standard protocols of single component exponential decay as shown below[3,4]. Briefly, a small circular region of the membrane was bleached for approximately ~3-5 seconds for the NBD dye and ~10-30 seconds for the Lyssamine Rhodamine Dye at 100% laser power. Fluorescence recovery was imaged over the course of 5-10 min.

FRAP data were fit to a single component decay model. The equation used was:

$$F(t) = A(1 - exp^{-t\tau}) \quad (1)$$

Where A is the recovery intensity of the mobile fraction as $t \rightarrow \infty$, generally bounded with a lower limit of last recorded intensity, τ is the characteristic diffusion time and t is the time at which intensity was recorded. The diffusion constant was then calculated using a previously published equation[3].

$$D = \frac{0.88 * \omega^2}{4\tau_{1/2}} \quad (2)$$

ω is the radius of the circular bleach region and the half-life, $\tau_{1/2}$, was calculated using equation 3 for single component exponential decay[4].

$$\tau_{1/2} = \frac{LN(0.5)}{-\tau} \quad (3)$$

These equations were used to fit the data seen in Figure S4.

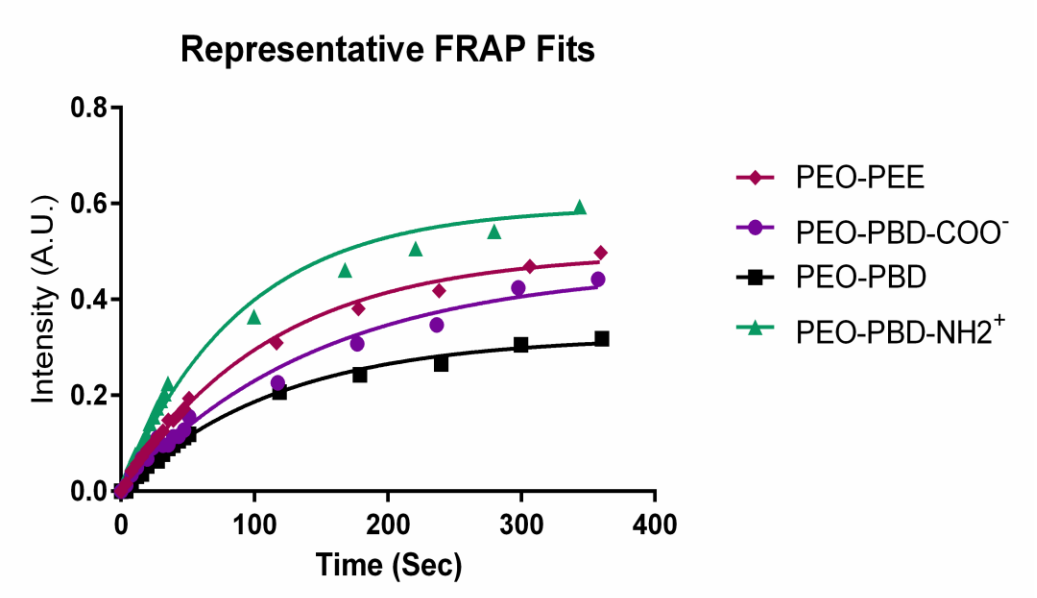

Figure S4. Fluorescence recovery after photobleaching raw data and fits for one representative data set on each polymer type. Each FRAP was fit to a single exponential equation (see methods for further explanation). The lines represent the fit of the real data points of the corresponding color.

Fluoresce recovery from a data set of polymer type PEO-PBD was used to compare additional diffusion recovery models[4-8]. The models are summarized in Tables S3 and S4 where each fit is evaluated based on mobile fraction and R-square value. Soumpasis et al. 1983 proposed,

$$F(t) = A * exp^{\frac{-\tau}{2t}}\left[I_0\left(\frac{-\tau}{2t}\right) + I_1\left(\frac{-\tau}{2t}\right)\right] \quad (4)$$

$$D = \frac{\omega^2}{\tau} \quad (5)$$

Where I_0 and I_1 are modified Bessel functions of first kind of 0 and 1st order respectively.[4] Equation 4 was utilized to calculate the characteristic diffusion time, τ, followed by equation 5 to calculate the diffusion constant. Equation 4 was also slightly modified by multiplying the first order Bessel function by the decaying exponential of the absolute value of the input vector. This is annotated in the tables as modified Soumpasis. Similar to the liposome gel rehydration FRAP analysis[1], the Feder et al 1996 diffusion model was investigated.

$$F(t) = \frac{F_0 + A\left(\frac{t}{\tau_{1/2}}\right)^{\alpha}}{1 + \left(\frac{t}{\tau_{1/2}}\right)^{\alpha}} \quad (6)$$

F_0 indicates the intensity after photobleaching, A is still the recovery intensity of the mobile fraction and α is the time exponent. By fitting A and the half-life, $\tau_{1/2}$, equations 7,9, and 10 were used to calculate characteristic time, τ, the transport coefficient Γ, and the diffusion coefficient.[5-6]

$$\tau = \frac{\tau_{1/2}}{\beta} \quad (7)$$

β is and empirical parameter bounded by $1<\beta<2$.[7] Both extremes of the β were evaluated in calculating the characteristic time and the subsequent diffusion constant as annotated in Tables S3 and S4.[5-7] The diffusion coefficient is expressed as

$$D = \frac{\Gamma t^{\alpha-1}}{4} \quad (8)$$

where Γ is the transport coefficient and is defined by:

$$\Gamma = \frac{\omega^2}{\tau^{\alpha}} \quad (9)$$

If the time exponent, α, is equal to 1 then the recovery follows Brownian diffusion, and by substituting for the transport coefficient, equation 8 reduces to equation 10.[6] In using this model, α, was found to be equal to 1.

$$D = \frac{\omega^2}{4\tau} \quad (10)$$

Initially, this method did adequately fit longer recovery profiles as F_0 was not recorded immediately after bleaching for the longer recovery data sets. To improve the evaluation of longer recovery profiles, F_0 was evaluated as a fitting parameter with the first recorded intensity used as an upper limit.

The final diffusion model investigated was derived from Jonsson et al 2008 utilizing Hankel transforms. Determining diffusion coefficient for this method was achieved using the frap analysis MATLAB software developed by Jonsson et al. and fitting equation 11.

$$F(k,t) = F(k,0)\left[(1-\gamma_2-\gamma_0)\, exp^{-4\pi^2k^2D_1t} + \gamma_2 exp^{-4\pi^2k^2D_2t} + \gamma_0\right] \quad (11)$$

D_1 and D_2 are diffusion coefficients if multiple diffusing components are selected within the program. Immobile fractions of each component are represented by γ_0 and γ_2. The Hankel transform at time = 0 and the spatial frequency from the Hankel transform are denoted F(k,0) and k respectively. A single component with and without an immobile

fraction was applied for determining the diffusion coefficient of the pGVs. The spatial frequency chosen for modeling is denoted in Table S3 and S4 and was selected following parameter guidelines[8].

Model	Mobile Fraction (%)	Diffusion Constant	R-square
Single Decay	32.27	0.011	0.996
Soumpasis	100	0.0087	0.959
Modified Soumpasis	38.19	0.015	0.986
Feder: β=1	44.64	.0066	0.997
Feder: β=2	44.64	0.013	0.997
Jonsson: s	N/A	0.0055	0.964
Jonsson: s+i	30.10	0.027	0.987

Table S3: Correlation table of single component decay model and diffusion model for 5 minute fluorescent recovery for PEO-PBD. β are empirical parameters for the Feder model.[5,7] Single component denoted as 's' and single component + immobile fraction denoted as 's+i' were both calculated for the Jonsson model. Single component modeling of the Jonsson method does not provide a mobile fraction. The max spatial frequency used for the Johnsson model was k=0.071 μm^-1 per fitting guidelines.[8] The Soumpasis and Johnsson models deviate the most given estimated mobile fraction, diffusion constant and R-square value.

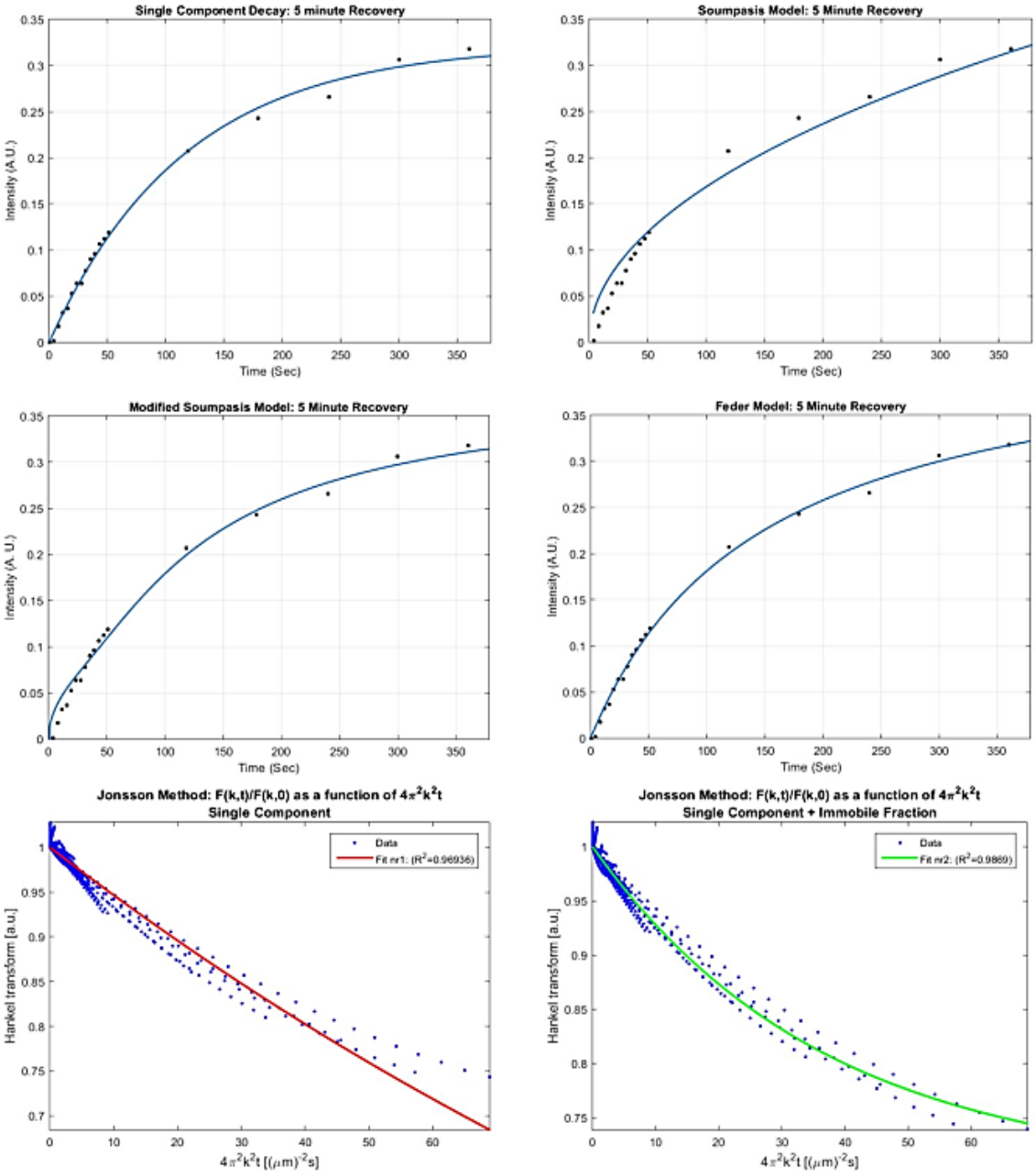

Figure S5. Representative graphs of single component decay model and diffusion model for 5 minute fluorescent recovery for PEO-PBD. The max spatial frequency used for the Johnsson model was k=0.071 μm^-1 per fitting guidelines.[8] The Soumpasis and Johnsson models deviate the most given estimated mobile fraction, diffusion constant and R-square value.

Model	Mobile Fraction (%)	Diffusion Constant	R-square
Single Decay	65.83	0.011	0.971
Soumpasis	91.76	0.0064	0.981
Modified Soumpasis	69.50	.022	0.978
Feder: β=1	77.89	0.010	0.985
Feder: β=2	77.89	0.020	0.985
Jonsson: s	N/A	0.014	0.971
Johnsson: s + i	71.41	0.026	0.984

Table S4: Correlation table of single component decay model and diffusion model for 10 minute fluorescent recovery for PEO-PBD. β are empirical parameters for the Feder model.[5,7] Single component denoted as 's' and single component + immobile fraction denoted as 's+i' were both calculated for the Jonsson model. Single component modeling of the Jonsson method does not provide a mobile fraction. The max spatial frequency used for the Johnsson model was k=0.075 μm^-1 per fitting guidelines.[8] The Soumpasis and Johnsson deviate the most given estimated mobile fraction, diffusion constant and R-square value.

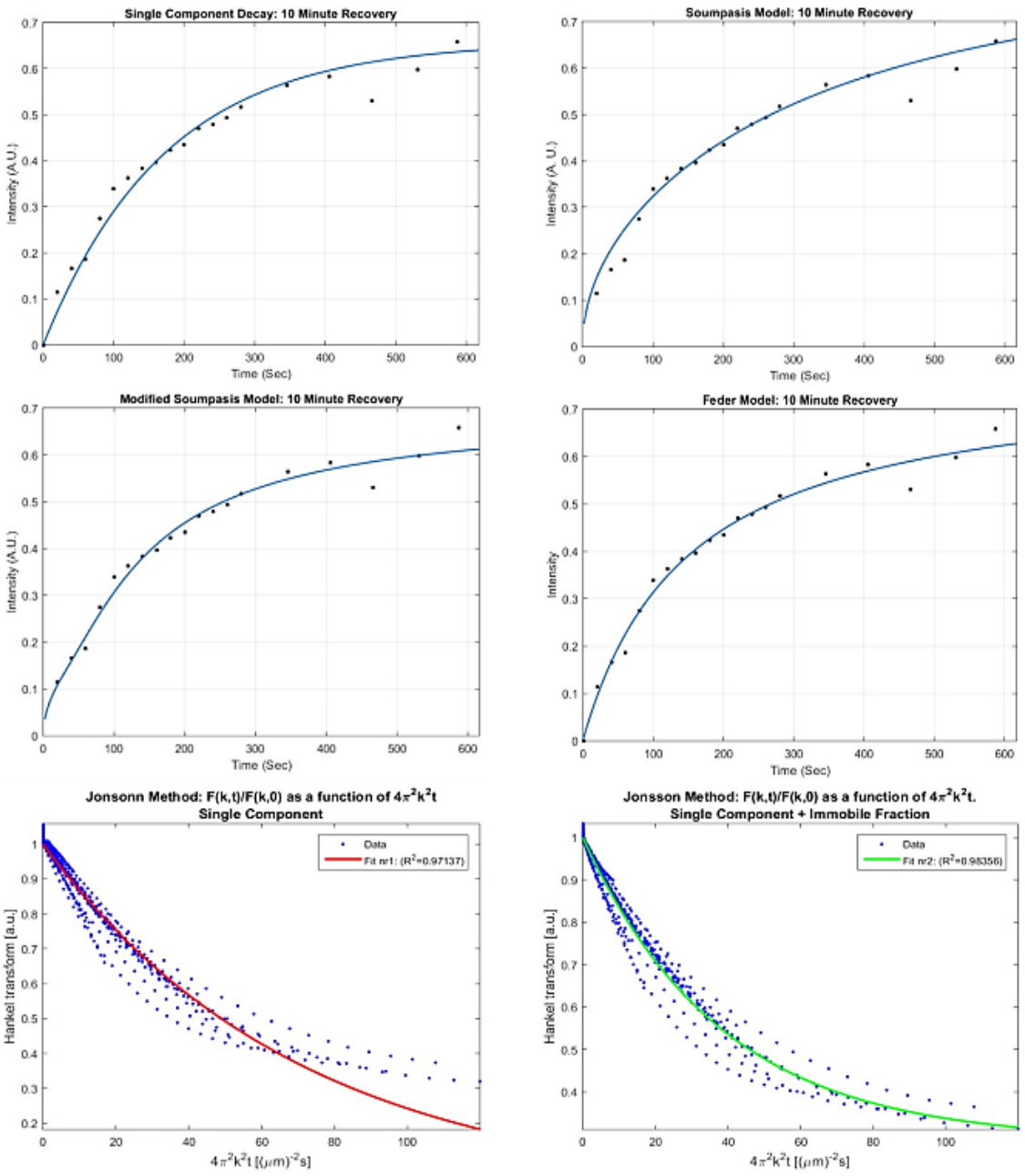

Figure S6. Representative graphs of single component decay model and diffusion model for 5 minute fluorescent recovery for PEO-PBD. The max spatial frequency used for the Johnsson model was k=0.071 μm^-1 per fitting guidelines.[8] The Soumpasis and Johnsson models deviate the most given estimated mobile fraction, diffusion constant and R-square value.

Sucrose-assisted rehydration

Formation of *p*GUVs was compared across the following four conditions: 1) 1% (w/w) agarose gels formed in water and PEO-PBD polymers rehydrated using deionized water, 2) 1% (w/w) agarose gels formed in water and PEO-PBD polymers rehydrated using 100mM sucrose (Figure S4A), 3) 1% (w/w) agarose gels formed in a 100 mM sucrose solution and PEO-PBD polymers rehydrated using deionized water and 4) 1% (w/w) agarose gels formed in a 100 mM sucrose solution and PEO-PBD polymers rehydrated using a 100 mM sucrose solution (Figure S4B). Polymersome diameter was measured using Fiji imaging software and size distributions were plotted using GraphPad Prism statistics software (La Jolla, CA). Two-way analysis of variance (ANOVA) analysis was performed using SigmaPlot (San Jose, CA).

Polymers of different molecular weights were deposited onto 1% (w/w) agarose gels and rehydrated with either deionized water or 100 mM sucrose (Figure S5). The addition of sucrose assisted in the formation of polymersomes compared to a simple rehydration in water. See main text for further discussion on the role of sucrose in the formation of *p*GUVs.

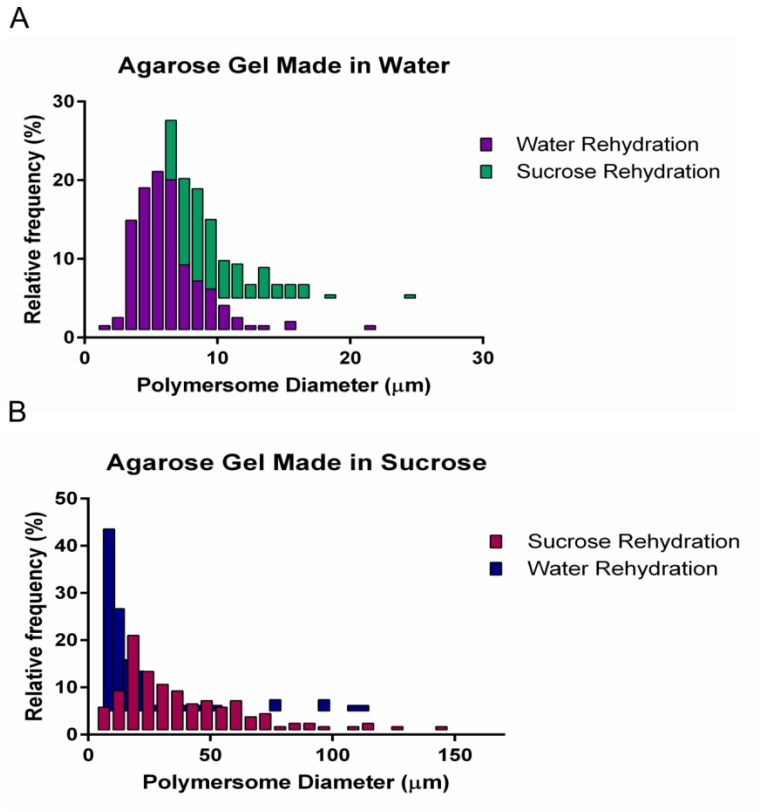

Figure S7. Addition of sucrose during the rehydration process increases PEO-PBD polymersome GUV size. (A) Percent frequency distribution of polymersomes made on water-based agarose gels and rehydrated with the indicated solutions. (B) Percent frequency distribution of polymersomes made on sucrose-based agarose gels and rehydrated with the indicated solutions. Note the differences in the x-axis scale.

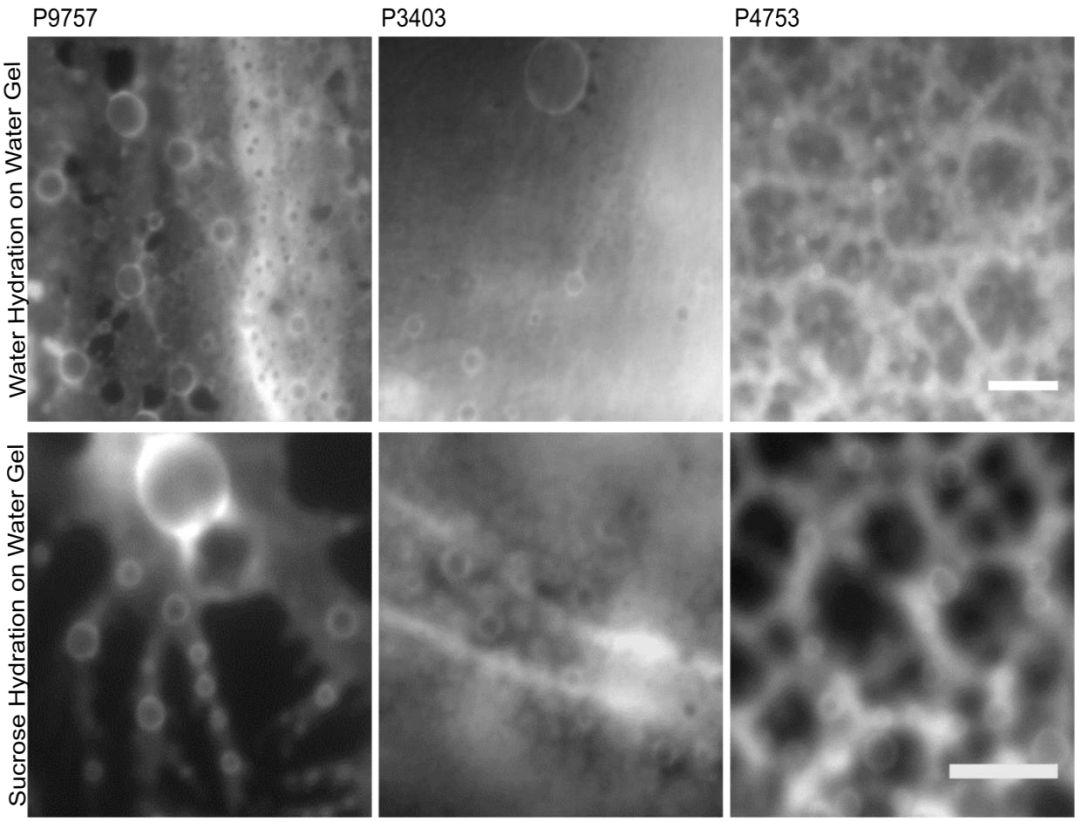

Figure S8. PEO-PBD polymersome GUV formation with different molecular weight polymers and different sucrose conditions. Epifluorescence images show that addition of sucrose successfully forms polymersome with polymers that typically do not form vesicles or do not robustly form vesicles. Scale bar is 10 µm.

.

References

[1] K. S. Horger, D. J. Estes, R. Capone, M. Mayer, **2009**, 2973–2982.

[2] J. Schindelin, I. Arganda-Carreras, E. Frise, V. Kaynig, M. Longair, T. Pietzsch, S. Preibisch, C. Rueden, S. Saalfeld, B. Schmid, et al., *Nat. Methods* **2012**, *9*, 676–82.

[3] D. Axelrod, D. E. Koppel, J. Schlessinger, E. Elson, W. W. Webb, *Biophys. J.* **1976**, *16*, 1055–1069.

[4] Soumpasis, D. M. *Biophys. J.* **1983**, 41, 95

[5] Feder, T. J.; Brust-Mascher, I.; Slattery, J. P.; Baird, B. Webb, W.W. *Biophys. J.* **1996**, 70, 2767.

[6] Bouchand, J.P.; Georges, A. *Phys Reports.* **1990**, 195, 127.

[7] Yguerabide, J., J. A. Schmidt, and E. E. Yguerabide. *Biophys. J.* **1982**, 39:69-75.

[8] P. Jönsson, M. P. Jonsson, J. O. Tegenfeldt, F. Höök, *Biophys. J.* **2008**, *95*, 5334–5348.

CHAPTER 2

Self-assembly and dynamic pH response of dual hydrophilic PEO-PAA vesicles

Preface

Self-assembly and dynamic pH response of dual hydrophilic PEO-PAA, represents collaborative work with co-first author Ian Henderson. Characterization of this unique vesicle forming dual hydrophilic diblock polymer is important to the work of creating a soft-matter hybrid delivery system because it provides a mechanistic study of how the polymeric coating might behave coupled to a particle system when exposed to environmental stimuli.

Abstract

We demonstrate the unique ability to self-assemble poly(ethylene oxide)-*b*-poly(acrylic acid) (PEO-PAA) into vesicles using only acidic or basic conditions and no additional molecular additives. Giant vesicles were formed vial gel rehydration at acidic conditions, pH 2-4, and pearl-like vesicle and vesicle clusters were produced in neutral to basic conditions, pH 6-12. Vesicle formation in the nanometer range is also achieved using simple film rehydration off of glass. A dynamic structural response was observed in both raising and lowering the pH of preformed PEO-PAA. Lastly, we provide a mechanism explaining vesicle structural variation and pH response based on and interchangeable block orientation driven by hydrophilic changes in the outer corona.

Introduction

Polymersomes are self-assembled membrane vesicles from amphiphilic polymers consisting of a hydrophilic inner/outer corona and hydrophobic membrane[1–4]. Structural formation into micelles, worm-like micelles, or vesicles is largely dependent on the geometric packing parameter dictated by the diblock hydrophilic fraction: $f_{\text{hydrophilic}}$[2,4,5]. Typically, polymersome morphology can be predicted with a $f_{\text{hydrophilic}} \approx 35 \pm 10\%$[2,4] , but it has been previously noted that this empirical rule is widely dependent on copolymer composition and solvent environment [5]. Both polymersomes and polymeric micelles can be uniquely tailored as "smart" response systems and are rapidly being implemented as nanocarriers for therapeutic delivery and diagnostics [5–7]. Alterations to both the type of copolymer and surface functionalization leads to limitless tunability for responses to pH, ions, temperature, ultrasound, magnetization, or light[3,6,8].

Out of all the vast formulations of self-assembly block copolymers from customary hydrophilic/hydrophobic diblock polymersomes to janus polymersomes[9,10], two very unique classes are "schizophrenic" diblock polymers and dual hydrophilic diblock polymers. "Schizophrenic" diblock polymers are described to have interchangeable core-corona or membrane-corona morphologies dependent on changes of pH, tempt, etc.[11–19] Dual hydrophilic copolymers such as poly(ethylene oxide)-b-poly(acrylic acid) (PEO-PAA) are intriguing as they can still self-assemble despite having no apparent hydrophobic block. Diblock copolymers consisting of PEO and PAA are particularly interesting for potential use in biomedical applications as PEO is renowned for its biocompatibility and stealth [5,20,21] in in-vivo systems and the pH responsiveness of PAA is well understood due to the carboxylate functional groups[20,22–

[26]. To our knowledge, the only PEO-PAA vesicle formation was recently achieved at pH10 conditions and self-assembly only occurred in the presence of α-cyclodextrin[27]. Under these conditions the α-cyclodextrin complexed with the PEO to change the hydrophilicity to form the hydrophobic membrane while the deprotonated carboxylic acids facilitated the PAA in forming the inner and outer corona[27]. Micellar formation of PEO-PAA has also been achieved using $Ca2^{+}$ at pH 9.7 consisting of a ionic stabilized PAA core and PEO hydrophilic region[28] Here we report the self-assembly of diblock copolymer PEO-PAA into polymersomes at various molecular weights in both basic and acid conditions using no molecular additives. Under the assumed mechanism of interchangeable corona block species; this diblock polymer exhibits variable pH formation and pH response.

Results and Discussion

As shown in Schematic 1, PEO-PAA was synthesized courtesy of Ian Henderson, using Atomic Transfer Radical Polymerization (ATRP) and click chemistry. Briefly, methyl acrylate (Acros) monomer was polymerized using and ATRP with a (1-Bromoethyl)benzene (Aldrich) initiator and a CuBr/PMDETA catalyst system in neat monomer to produce polymethacrylate (PMA). Polymer length was controlled by reaction time. After displacing the bromine end-group of the PMA with sodium azide, the PMA was attached to propargyl PEO (produced by the reaction of PEO(Fluka) with propargyl bromide (Aldrich)) through click chemistry producing PEO-PMA. Lastly, the methyl group of the PMA block was deprotected through KOH producing PEO-PAA. ATRP polymer production allows for controlled and reproducible molecular weight distribution [29–32] and customizable end-chain functionality[30–32] for use in additional

processes. Furthermore, ATRP is widely used to produce other pH sensitive block polymers as nanocarriers[20,33,34] and other dual hydrophilic polymers [28,35,36]. Precision molecular control is vital in effective reproduction of polymer vesicles and this processes is further supplemented through the simplicity of diblock coupling via click chemistry[37,38]. This synthesis technique produced variable weights of the dual-hydrophilic diblock polymer of: PEO_{750}-PAA_{950} (1.7kDa, EO_{17}-AA_{12}), PEO_{2000}-PAA_{3000} (5kDa, EO_{45}-AA_{38}), and PEO_{5000}-PAA_{3000} (8kDa, EO_{114}-AA_{38}).

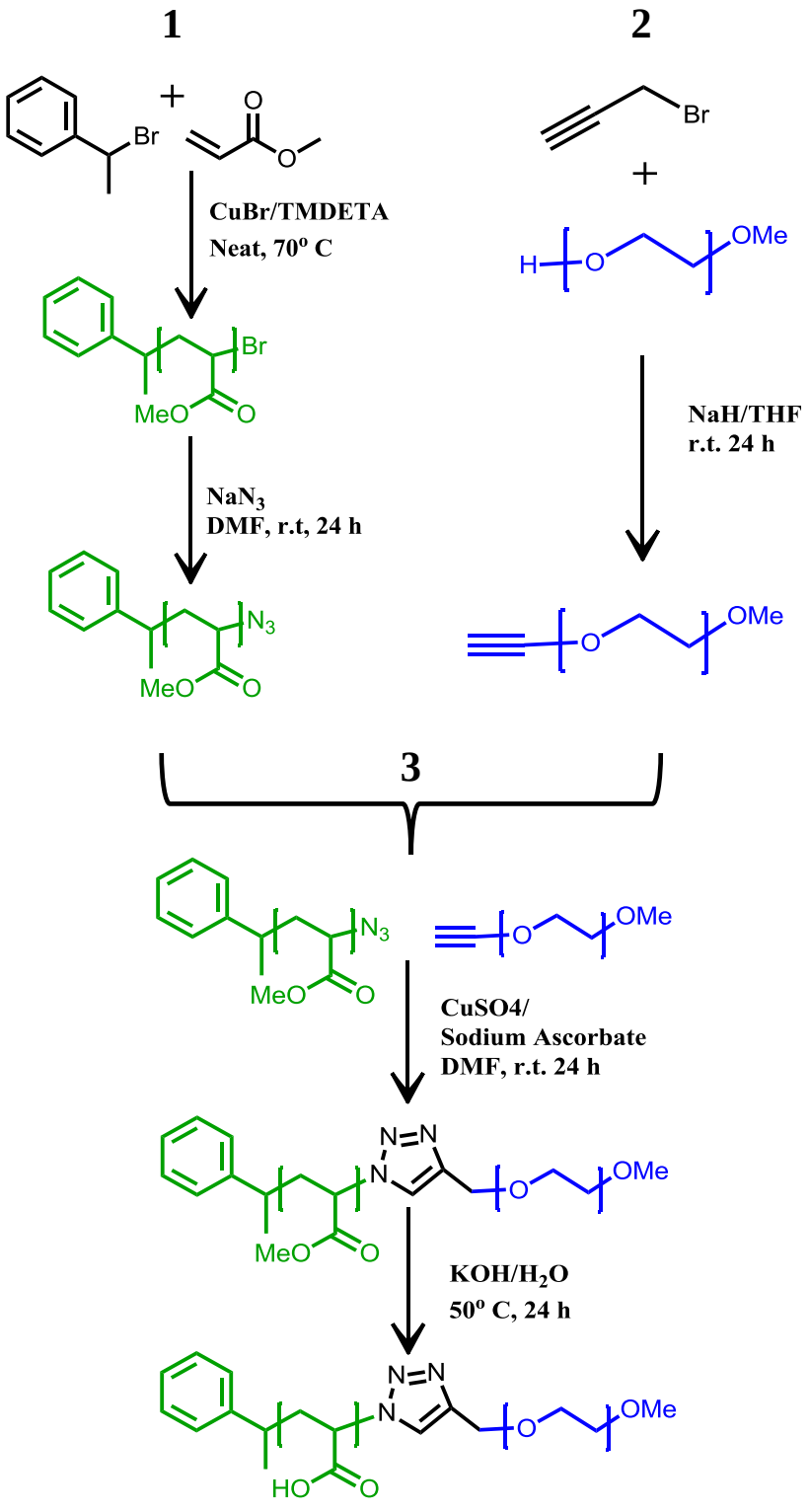

Scheme 1. Schematic depicting PEO-PAA synthesis as described in text.

Using gel-assisted rehydration, pGVs were formed at all molecular weights. 5kDa PEO-PAA pGVs formed vesicles at acidic conditions pH2-4, where pearl-like vesicles and vesicle clusters were observed at pH6-12 (Figure 1). Formation in neutral-basic pH initially appeared to have dominant morphologies of pearls, clusters, or multilamellar vesicles at the varying pHs (Figure S1), but repeat studies revealed stochastic trends that are currently under investigation. Polymersomes at acidic conditions most likely consist of a PAA hydrophobic membrane due to the protonation of carboxylate groups, pKa ~4.5[39,40] which give an $f_{\text{hydrophilic}}$ approximately 40%. During formation at neutral-basic formation, the corona is postulated to comprise of PAA instead of PEO due ionization of the PAA block, f_{AA} = 60%. Similarly, vesicle formation was seen with 1.7kDA PEO-PAA with preferential vesicle formation in acid conditions, $f_{EO} \approx 44\%$ (Figure 2). The lower molecular weight PEO-PAA polymersomes also decreased in sphericity, lamellarity, and vesicle density with increasing pH, which is reflected in the structural variations (Figure S2). Lastly, 8kDa PEO-PAA produced vesicles at pH 2, $f_{EO} \approx$ 63%, where almost nothing was observed at pH 12 $f_{AA} \approx 37\%$ (Figure 3). The 1.7kDa and 5kDa PEO-PAA hydrophilic fraction fall on the outer edge of predicative vesicle formation, but the 8kDA PEO-PAA has a significantly larger hydrophilic block fraction. Clearly this dual-hydrophilic block polymer falls outside the empirical rule of predictive structures from the hydrophilic block fraction.

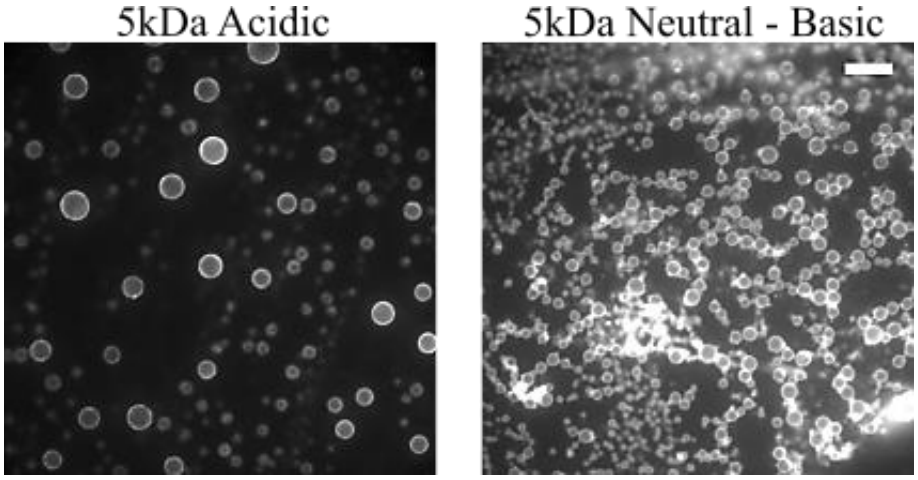

Figure 1. 5Kda PEO-PAA pGV formation at pHs 2,4,6,8,10,12. pH 2 and 4 exhibited similar structural dynamics of vesicle formation where as pH6-12 formed pearl-like structures and vesicle clusters. Used 100x objective and scale bar is set at 10μm.

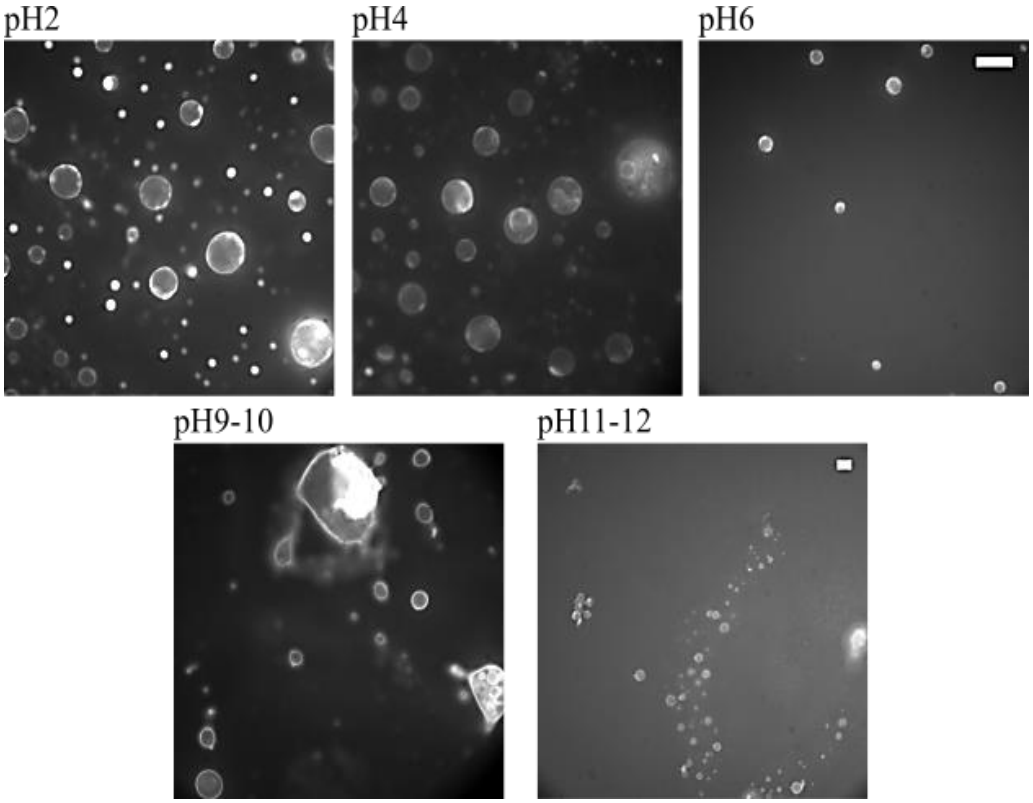

Figure 2. 1.7kDa PEO-PAA pGV formation at pHs 2,4,6,9-10, 11-12. pH 2 formation shows domain segregation where higher pH produced variable self-assembly structures. pH2,4,6 and 9-10 were imaged with 100x objective corresponding to 10μm scale bar displayed in pH6 image. pH11-12 was imaged at 40x displayed with 10μm scale bar.

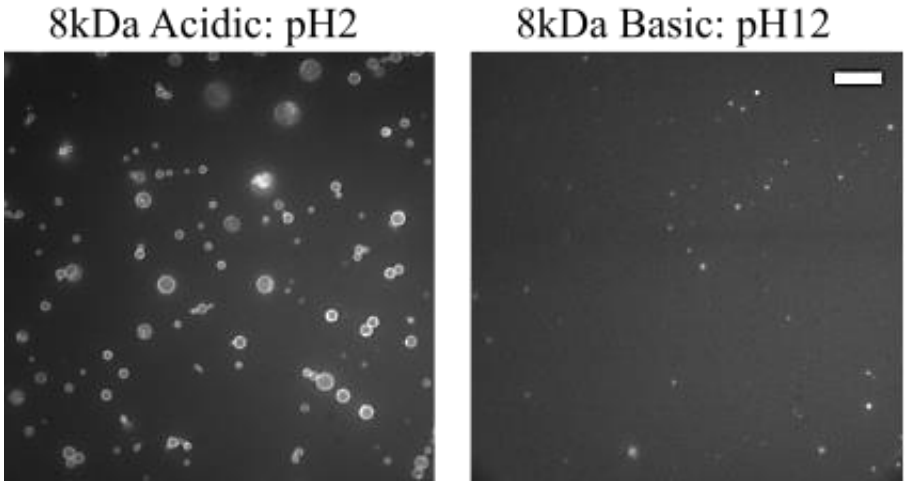

Figure 3. 8kDa PEO-PAA pGV formation at pHs 2 and 12 imaged with 100x objective. pH 2 successfully made polymersomes where almost no formation was seen at pH12. Scale bar is set at 10μm from images taken at 100x objective.

The variable self-assemble structures is not too surprising given that a dual-hydrophilic can most likely express variable degrees of hydrophilicity given environmental conditions. Supplementary to the distinctive self-assembly classes, this PEO-PAA also exhibits a pH response. Preformed 5kDa vesicles at pH2 degrade over time when exposed to 36μmoles of sodium hydroxide (NaOH) (Figure 4). This is evident in loss of surface density overtime, and though some of the population may be losing adherence to gel, degradation is more likely due to diffusion of dye from damaged polymersomes. Moreover, there was no polymersomes observed when the rehydration media was harvested off the gel, but additional studies are underway to verify if any vesicle species exist in the solution suspended above the gel when alkalized (Figure S3).

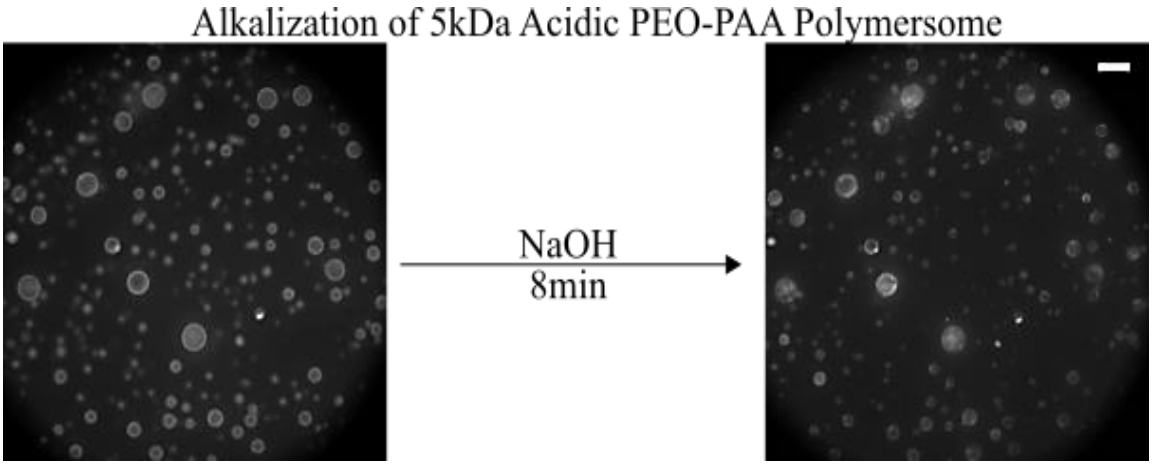

Figure 4. 5kDa PEO-PAA polymersome formation at pH2 exposed to 36µmoles of NaOH. Density decreases overtime as well as structural integrity of polymersome. Scale bar is set at 10µm from images taken at 100x objective.

Similarly, 1.7kDa acidic polymersomes display membrane disruption and disassembly under the same basic conditions (Figure S4). A higher degree of disassembly is observed in the 1.7kDa structures compared to the 5kDa vesicle (Figure S4 and S5), which is expected as the higher molecular weight can withstand higher degrees of tension[4]. Poly(ethylene oxide)-*b*-poly(butadiene) (PEO_{950}-PBD_{2000}, EO_{22}-BD_{37}, Polymer Source, Inc.) was used as a control and formed at pH2 before alkalized with 36µmoles of NaOH (Figure S6). Surface loss is also seen in the alkalization of PEO-PBD vesicles; however the same dynamics are not present as previously described with the PEO-PAA vesicles. In order to rule out osmotics, acidic polymersomes were subjected to 36µmoles of monovalent NaCl, 100µM and 1mM of $CaCl_2$ (Figure S7). Long term stabilization was witnessed over a period of 8 hours ruling out the pH effect being attributed to osmotics. Despite the presence of screening salts, acid PEO-PAA polymersomes exhibit the same interesting transient behavior (Figure S8) and long term response (Figures S9) of system degradation when treated with NaOH.

Complimentary to the alkalization response of acidic PEO-PAA polymersomes, basic PEO-PAA polymersomes also demonstrate a pH response to acidification. Pearl-like vesicles formed at pH12 with 5kDa PEO-PAA exhibit structural rearrangement when treated with 36μmoles of HCl (Figure 5). Upon addition of the acid, the PAA block (currently in the corona) becomes increasingly protonated, and therefore hydrophobic. As protonation occurs, the membranes of the pearls interdigitate with each other, leading to hydrophobically driven fusion of the pearls into large vesicles. Presumably, at the time of fusion, the membrane also undergoes inversion so that the resulting vesicles contain a PEO corona and a protonated PAA-hydrophobic wall.

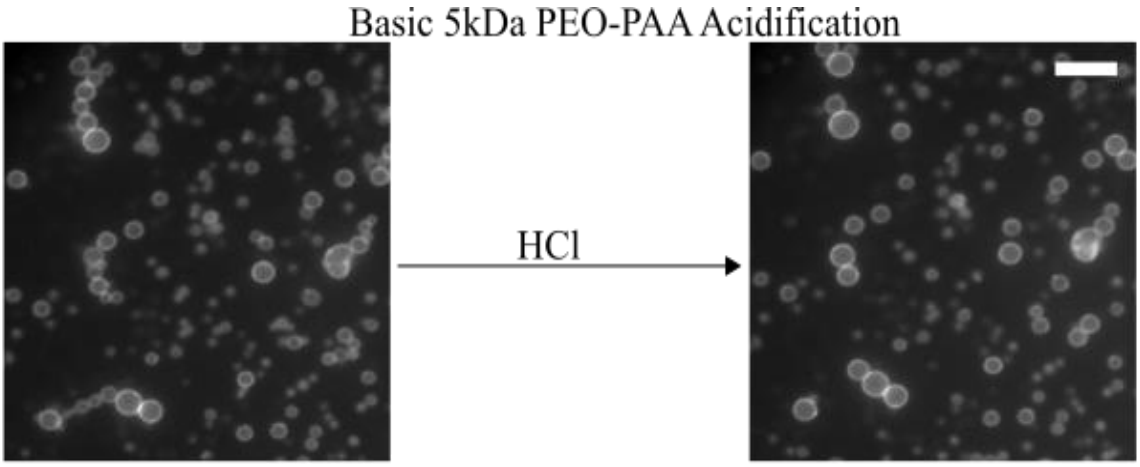

Figure 5. 5kDa PEO-PAA polymersome formation at pH12 treated with 36μmoles of HCl. Fusion occurred over 50 seconds. Scale bar is set at 10μm from images taken at 100x objective.

Interestingly, pearl-vesicles formed in DIH20, pH6.2 also fuse when exposed to acid (Figures S10). Even though self-assembly varies at that pH, it is not unexpected that PAA would still dominate in the outer corona. A control of PEO-PBD was also formed at PH12 and did not exhibit the structural dynamics or pH response (Figure S10) further substantiating the ability and assembly modality of the PEO-PAA copolymer.

Formation of the large dual hydrophilic structures has proved invaluable in characterizing this dual responsive polymer, and by using thin film hydration, nanostructures were developed from the 1.7kDa block weights (Figures S11-S13). The vesicle formation from the thin film hydration before processing to produce nano-assemblies provides strong evidence that after sonication and filtration, nano-polymersomes are formed. At this scale the PEO-PAA demonstrates an equal response to acidification and alkalization (Figures S12-13) as seen in the gel system.

We have demonstrated the formation of a dual hydrophilic block copolymer that is independent of any molecular additives. pH driven self-assembly, disassembly, and rearrangement, coupled with molecular weight dependent formation, supports the mechanism of a reversible corona species. In addition with the production of large-scale structures, we have strong evidence of nanometer vesicle production with the same pH dynamics. This system can be applied for many biomedical applications due to the distinct response to both acidification and alkylation and the "stealth" characteristics of the PEO block. There is no boundary for controlled delivery in gastro-intestinal studies or endosomal release.

References

[1] S. Rangelov, S. Pispas, *Polymer and Polymer-Hybrid Nanoparticles: From Synthesis to Biomedical Applications*, **2014**.

[2] D. E. Discher, A. Eisenberg, *Science* **2002**, *297*, 967–973.

[3] G.-Y. Liu, C.-J. Chen, J. Ji, *Soft Matter* **2012**, *8*, 8811.

[4] D. E. Discher, F. Ahmed, *Annu. Rev. Biomed. Eng.* **2006**, *8*, 323–341.

[5] R. P. Brinkhuis, F. P. J. T. Rutjes, J. C. M. van Hest, *Polym. Chem.* **2011**, *2*, 1449.

[6] F. Meng, Z. Zhong, J. Feijen, *Biomacromolecules* **2009**, *10*, 197–209.

[7] W. Chen, J. Du, *Sci. Rep.* **2013**, *3*, 2162.

[8] W. Chen, F. Meng, R. Cheng, Z. Zhong, *J. Control. Release* **2010**, *142*, 40–46.

[9] D. a Christian, A. Tian, W. G. Ellenbroek, I. Levental, K. Rajagopal, P. a Janmey, A. J. Liu, T. Baumgart, D. E. Discher, *Nat. Mater.* **2009**, *8*, 843–849.

[10] R. Deng, F. Liang, X. Qu, Q. Wang, J. Zhu, Z. Yang, *Macromolecules* **2015**, *48*, 750–755.

[11] R. Enomoto, M. Khimani, P. Bahadur, S. Yusa, *J. Taiwan Inst. Chem. Eng.* **2014**, *45*, 3117–3123.

[12] A. Feng, C. Zhan, Q. Yan, B. Liu, J. Yuan, *Chem. Commun.* **2014**, *50*, 8958.

[13] A. E. Smith, X. Xu, S. E. Kirkland-York, D. a. Savin, C. L. McCormick, *Macromolecules* **2010**, *43*, 1210–1217.

[14] X. Andre, M. Burkhardt, M. Drechsler, M. Gradzielski, A. H. E. Müller, I. M. V. L. Langevin, F.-G. France, **2007**, 560–561.

[15] S. Guragain, B. P. Bastakoti, K. Nakashima, *J. Colloid Interface Sci.* **2010**, *350*, 63–68.

[16] J. Rodríguez-Hernández, S. Lecommandoux, *J. Am. Chem. Soc.* **2005**, *127*, 2026–2027.

[17] D. Jianzhong, R. K. O'Reilly, *Macromol. Chem. Phys.* **2010**, *211*, 1530–1537.

[18] V. Butun, N. C. Billingham, S. P. Armes, *J. Am. Chem. Soc.* **1998**, *120*, 12135–12136.

[19] F. Liu, A. Eisenberg, *J. Am. Chem. Soc.* **2003**, *125*, 15059–15064.

[20] Q. Liu, J. Chen, J. Du, *Biomacromolecules* **2014**, *15*, 3072–3082.

[21] J. S. Lee, K. D. Park, **2011**, *15*, 152–158.

[22] V. V Khutoryanskiy, A. V Dubolazov, Z. S. Nurkeeva, G. a Mun, *Langmuir* **2004**, *20*, 3785–3790.

[23] a. K. Bajpai, S. K. Shukla, S. Bhanu, S. Kankane, *Prog. Polym. Sci.* **2008**, *33*, 1088–1118.

[24] S. Ganta, H. Devalapally, A. Shahiwala, M. Amiji, *J. Control. Release* **2008**, *126*, 187–204.

[25] K. Letchford, H. Burt, *Eur. J. Pharm. Biopharm.* **2007**, *65*, 259–269.

[26] N. Murthy, J. Campbell, N. Fausto, A. S. Hoffman, P. S. Stayton, *J. Control. Release* **2003**, *89*, 365–374.

[27] J. Liu, H. R. Sondjaja, K. C. Tam, *Langmuir* **2007**, *23*, 5106–5109.

[28] R. Sondjaja, T. a Hatton, K. C. Tam, *Langmuir* **2008**, 8501–8506.

[29] K. Dayananda, B. S. Pi, B. S. Kim, T. G. Park, D. S. Lee, *Polymer (Guildf).* **2007**, *48*, 758–762.

[30] K. Matyjaszewski, *Macromolecules* **2012**, *45*, 4015–4039.

[31] K. Matyjaszewski, N. V Tsarevsky, *Nat. Chem.* **2009**, *1*, 276–288.

[32] N. V Tsarevsky, K. Matyjaszewski, *Chem. Rev.* **2007**, *107*, 2270–2299.

[33] M. H. Dufresne, D. Le Garrec, V. Sant, J. C. Leroux, M. Ranger, *Int. J. Pharm.* **2004**, *277*, 81–90.

[34] J. Du, L. Fan, Q. Liu, *Macromolecules* **2012**, *45*, 8275–8283.

[35] R. Sondjaja, T. Alan Hatton, M. K. C. Tam, *J. Magn. Magn. Mater.* **2009**, *321*, 2393–2397.

[36] Z. Ge, J. Xu, D. Wu, R. Narain, S. Liu, *Macromol. Chem. Phys.* **2008**, *209*, 754–763.

[37] P. Thirumurugan, D. Matosiuk, K. Jozwiak, *Chem. Rev.* **2013**, *113*, 4905–4979.

[38] K. Nwe, M. W. Brechbiel, *Cancer Biother. Radiopharm.* **2009**, *24*, 289–302.

[39] Pradip, C. Maltesh, P. Somasundaran, R. a Kulkarni, S. Gundiah, *Langmuir* **1991**, *7*, 2108–2111.

[40] S. Kim, J. Y. Kim, K. M. Huh, G. Acharya, K. Park, *J. Control. Release* **2008**, *132*, 222–229.

[41] J. Schindelin, I. Arganda-Carreras, E. Frise, V. Kaynig, M. Longair, T. Pietzsch, S. Preibisch, C. Rueden, S. Saalfeld, B. Schmid, et al., *Nat. Methods* **2012**, *9*, 676–82.

Supporting Information

pGV Formation Method and pH Titrations

pGV formation was achieved through agrose gel-rehydration as explained in Chapter 1 with polymers prepped with 0.5 mol% Lissamine Rhodamine B PE lipid (Avanti Polar Lipids, Inc., Alabaster, AL). Prepping of pH solutions and titrations were done with either hydrochloric acid (HCl, Fisher) or sodium hydroxide (biological molecular grade NaOH, Fisher). pH measurements were carried out using Orion Ross ultra semi-electrode (8115BNUWP) and Orion Star A211 pH meter (Thermo Scientific). Imaging was carried out as described in Chapter 1, using Olympus IX81 in epifluorescence and an Orca-Flash 4.0 cMOS camera (Hamamatsu Photonics, San Diego, CA). Fiji imaging software was used to process the images[1].

Structural Formations of 5kDa PEO-PAA varying pHs

Acidic formation of 5kDa at pH 2, S1: tri-panel A, was dominated by polymersomes with some population of fused vesicles. Dynamics changed in neutral to basic pH that is currently under investigation due to fluctuating trends. Rehydration in DI H20, pH~6.2, resulted in unilamellar polymersomes, multilamellar polymersomes, and pearl structures, S1: tri-panel B. ph4 rehydration, tri-panel C, largely produced polymersome populations where currently pH 8 and 10, S1: tri-panel C were dominated by polymersomes clusters.

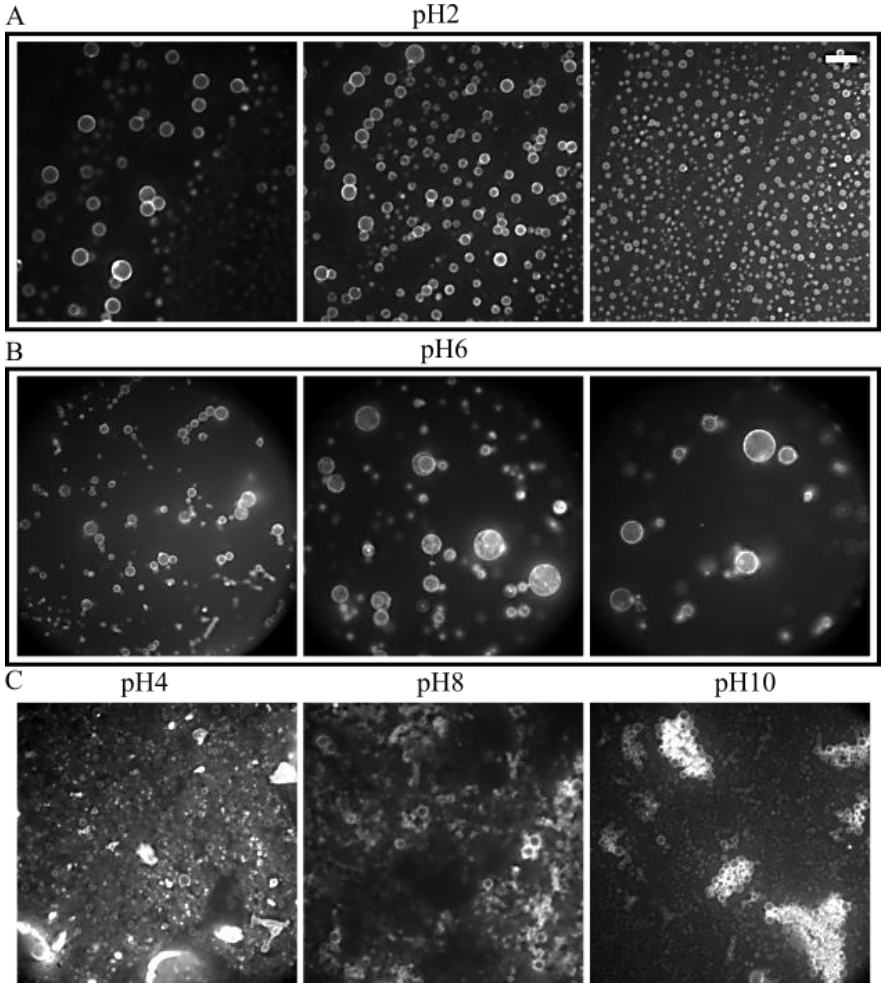

Figure S1. 5kDa formation dynamics at varying pHs. Acidic formation at pH 2,tri-panel A, produced mostly polymersomes. Structural dynamics changed in rehydration with DI H20 pH~6.2 producing single membrane polymersomes, multilamellar polymersomes, and pearl structures, tri-panel B. Similarly to pH 2, ph4, 8 and 10 rehydration, tri-panel C, exhibited preferential structure formation of polymersomes and vesicle clusters respectively. Scale bar is set at 10μm from images taken at 100x objective.

Structural Formations of 1.7kDa PEO-PAA varying pHs

Acidic formation at pH4 shows domain segregated, single membrane polymersomes and multilamellar polymersomes. pH2 dynamics are not shown as species dominance is accurately portrayed in Figure 2 of vesicles and domain segregated vesicles. pH 6, DIH20 rehydration, also did not have any variable formation due to low self-assembly density. Therefore, mostly polymersome formation was seen in sparse quantities at pH6. Ph9-10 and pH11-12 displayed vesicles and other larger agglomerate structures.

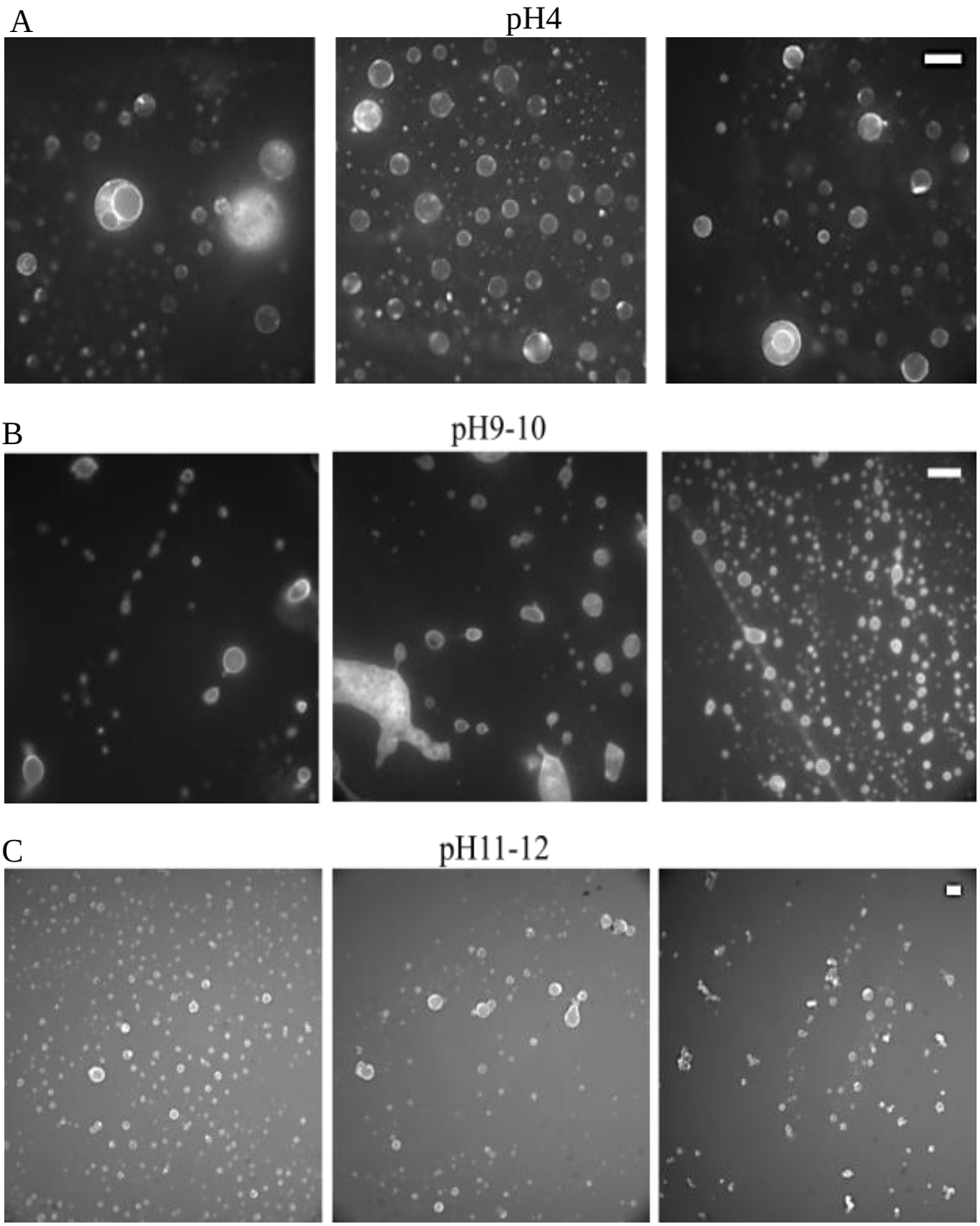

Figure S2. 1.7kDa formation dynamics at varying pHs. Each panel highlights structural variations at different pHs with: Panel A corresponding to pH4, Panel B corresponding to pH9-11 and panel C, corresponding to pH11-12. pH 2 and 6 formed one dominant self-assembly species and are not shown. All scale bars are expressed for each panel set at 10μm. Panel A and B were imaged at with a 100x objective and panel C was imaged with a 40x objective

Solution Examination of Alkalized PEO-PAA vesicles

Polymersomes that disappear from the field of view after NaOH addition have the potential of detaching from the surface before degradation. The image as shown in Figure S4 shows potentially large structures above the gel surface, but vesicles at 40x magnification should still be able to be distinguished. The rehydration solvent was also extracted in attempt to capture any free floating polymersomes but there was not a single event witnessed. Further investigation is being conducted, but given all the evidence membrane disruption and destruction is the most likely scenario.

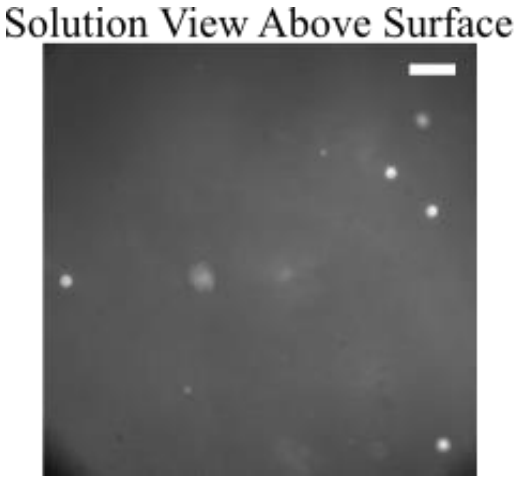

Figure S3. 5kDa 40x solution view above gel surface after addtion36 µMoles of NaOH.

Alkalized pH Response of 1.7kDa Acidic Polymersomes

Mirroring the alkalization pH Response of 5kDa acidic PEO-PAA polymersomes (Figure 4), 1.7kDa polymersomes degraded when adding NAOH, 36 µMoles. Loss of vesicle integrity is evident with progression of time and is complimented by diffuse and increased fluorescent intensity form escaped dye of previous self-assembled structures.

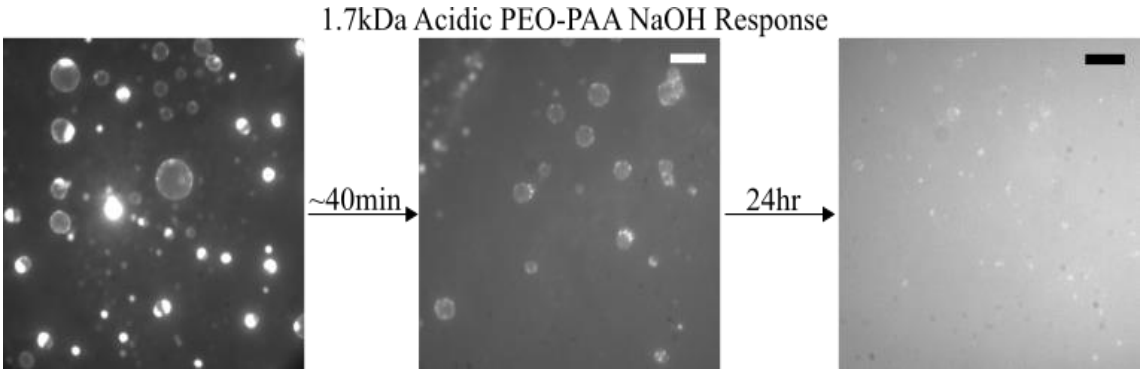

Figure S4. 1.7kDa pH response of acidic vesicles to addition of NaOH 36 µMoles. All scale bars are expressed at 10µm from imaging with 100x objective

Long Term Alkalized pH Response of 5kDa Acidic Polymersomes

During a 24 hour period, the vesicle population upon exposure to 36 µMoles of NaOH is in excess compared to the acidic 1.7kDa PEO-PAA polymersomes, but loss of vesicles is still evident. Response appears more severe with 1.7kda polymersomes which is warranted given that the increased molecular can withstand a higher degree of perturbations.

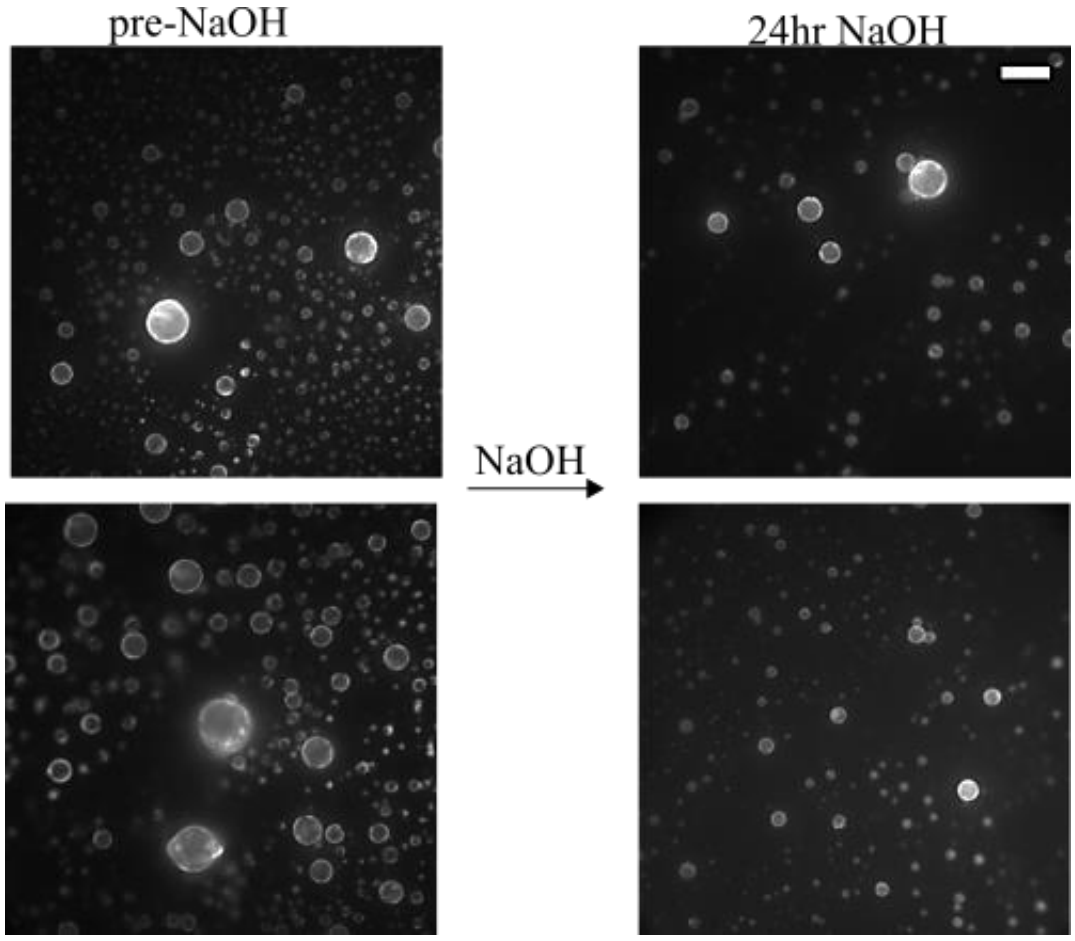

Figure S5. 5kDa 24 hour NaOH response. Scale bar is expressed at 10μm from imaging with 100x objective

Alkalinized pH Response of PEO-PBD

Poly(ethylene oxide)-*b*-poly(butadiene) (PEO_{950}-PBD_{2000}, EO_{22}-$BD_{37,}$ Polymer Source, Inc.) pGVs were formed in acid conditions at pH 2 as a control for NaOH response. PEO-PBD has a distinctive hydrophobic block PBD, and the hydrophilic block PEO has a $f_{EO} \approx 32\%$. pGV characteristics mimic PEO-PBD formation in buffer or media as shown in Chapter 1. Upon adding 36 μMoles of NaOH vesicles appeared to detach or burst from the surface almost immediately highlighted by the holes observed in Figure S3. pH response observed in the dual hydrophilic PEO-PAA is still believed to be valid

given that dye diffusion is not evident in the PEO-PBD sample. Also the transient or long term behavior seen in the PEO-PAA acid polymersome was not seen here. Determination of PEO-PBD polymersome fate upon alkalization requires further investigation that is currently underway.

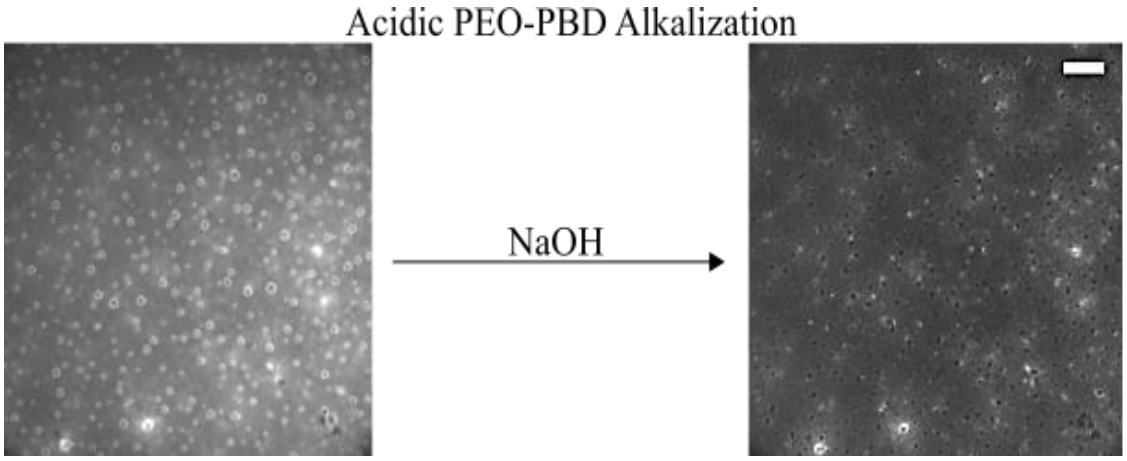

Figure S6. PEO-PBD pH2 polymersomes alkalized by 36 µMoles NaOH. 100x objective used and scale bar is set at 10µm.

Osmotic Study

Acidic polymersomes were subjected to monovalent salt NaCl (36 µMoles) and divalent salt, $CaCl_2$ (100µM and 1mM) to study any osmotic effect. 1mM Ca2+ exposure was monitored initially for 10 minute and no change was observed as seen in Figure S7. Additional verification of stability was conducted at 8 hours. 100µM Ca2+ and NaCl 10 minute monitoring (data not shown) revealed the same results.

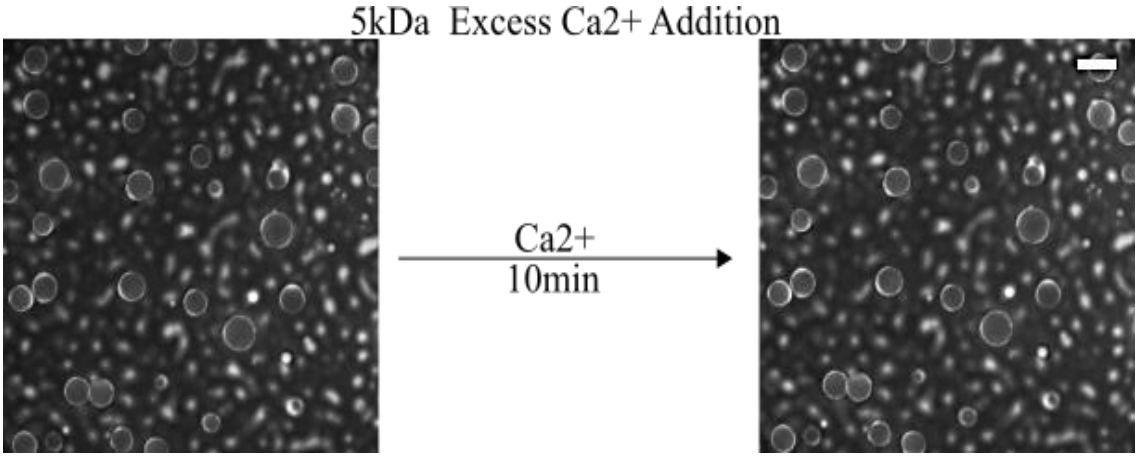

Figure S7. Acid 5kDa with exposure to 1mM Ca2+ shows no reaction and stability up to 8 hours. Image was taken at 100x objective with a scale bar of 10µm.

Base Response in the Presence of Salts

Acidic polymersomes still expressed both a transient response to alkalization, Figure S8 and a long term disassembly response, Figure S9, in the presence of screening ions of $CaCl_2$ (100µM). When 36µmoles of NaOH is added, the immediate disruption to the system is evident in the diffusion of debris and detachment of some vesicles as captured in Figure S8. This mimics the response when no salt is present. Monitoring the system over hours, Figure S9, shows the continual loss of polymersomes.

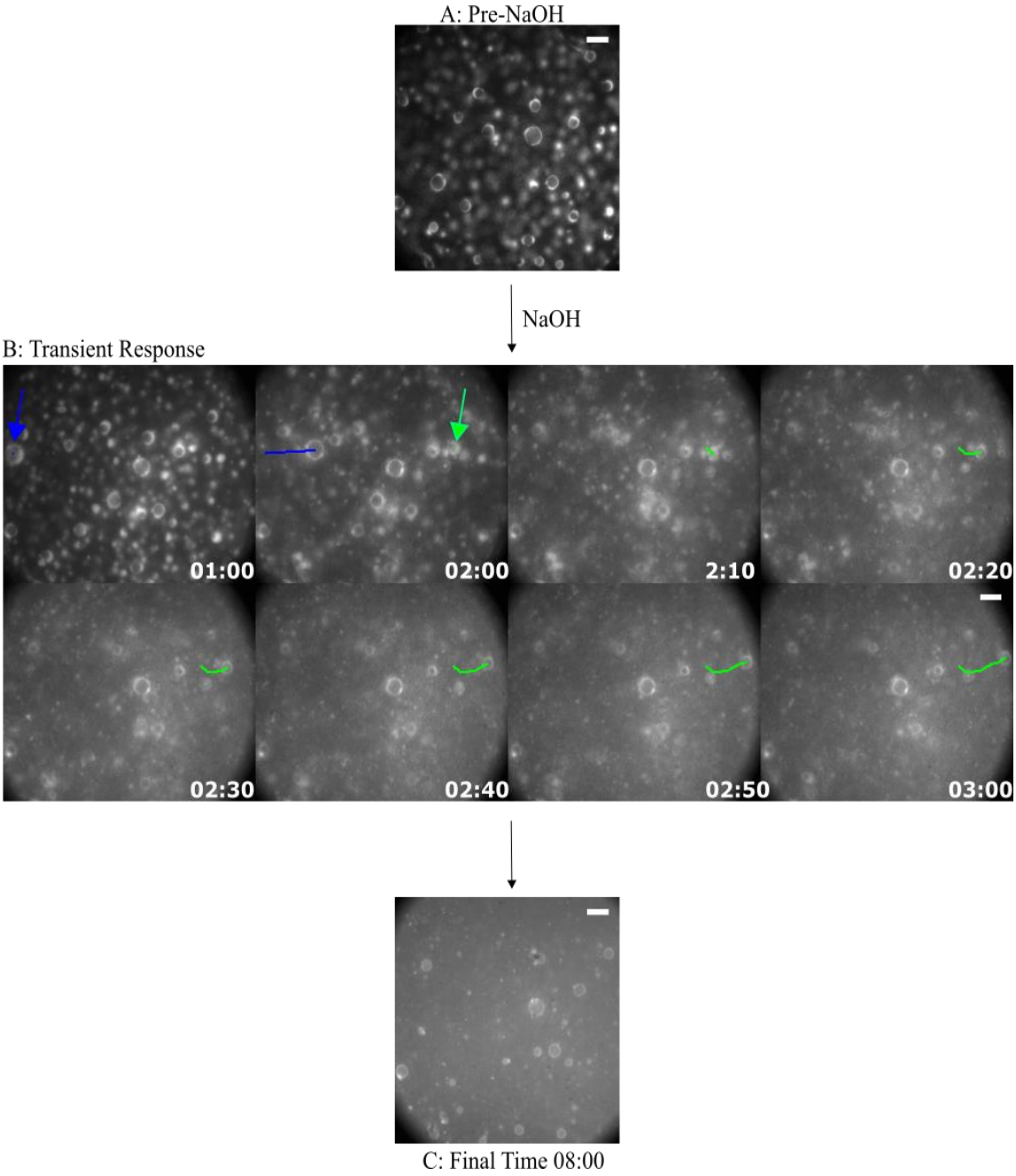

Figure S8. Transient behavior of alkalized acidic 5kDa polymersome in the presence of 100μM $CaCl_2$ screening salt. Image was taken at 100x objective with a scale bar of 10μm.

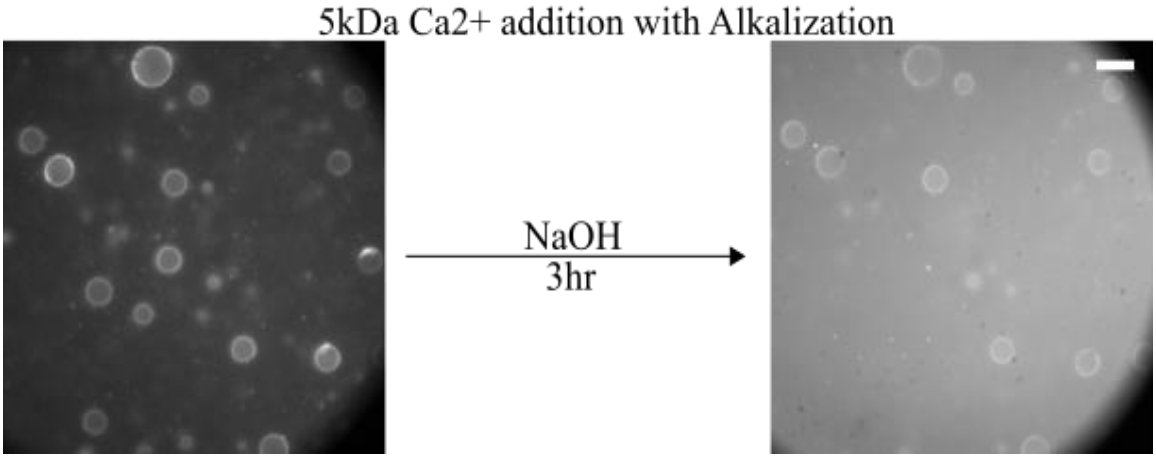

Figure S9. Long-term behavior of alkalized acidic 5kDa polymersome in the presence of 100μM $CaCl_2$ screening salt.

Acidification of Neutral 5kDa PEO-PAA and Basic PEO-PBD Polymersomes

5kDa PEO-PAA Polymersomes formed in DI water that exhibit dynamic structural variations (Figure S1) show the same fusion rearrangement response as basic polymersome when acidified. Polymer pearls fuse when exposed to 36μmoles of HCl. The fusions happened immediately over a course of ~40sec.

PEO-PBD, contain a distinct hydrophobic block that form large pGV structures at pH12 in contrast to the pearl-like vesicles and clusters seen in PEO-PAA formation. Initial system disruption and swelling of some events were observed when PEO-PBD vesicles were treated with 36μmoles of HCl, but overall the system remained unchanged as seen in Figure S10. Both the formation of PEO-PBD and lack of response to acidification substantiate the unique response of the dual hydrophilic PEO-PAA copolymer.

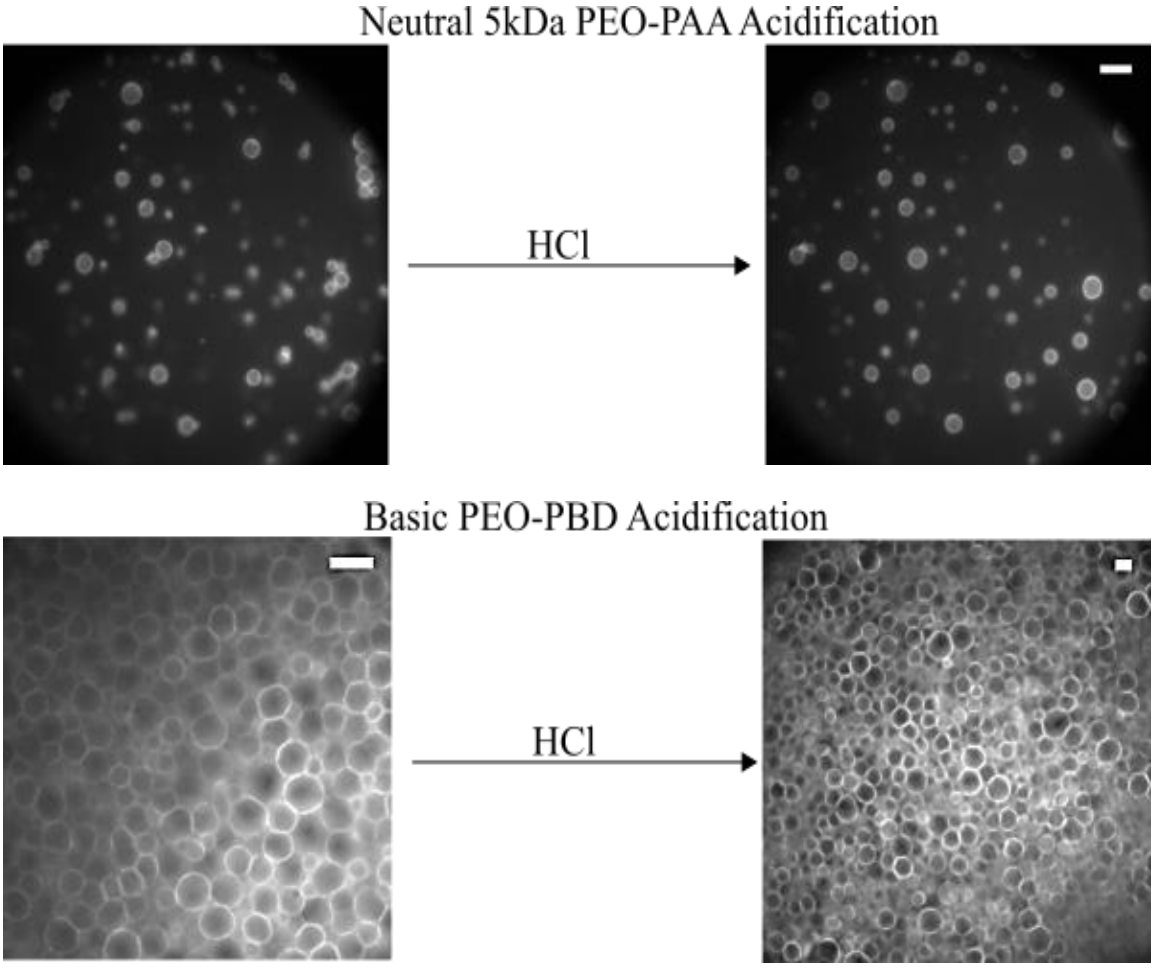

Figure S10. Neutral PEO-PAA 5kDa fusion response to acidification shown in the top panel imaged at 100x with scale bar set at 10μm. Acidification of pH12 formed PEO-PBD vesicles show no response with scale bars set at 10μm and imaged at 100x and 40x respectively.

Nanostructure Formation Method and pH Titrations

Thin film hydration was used to form vesicles or PEO-PAA nanostructures[2]. 1-5 mg of dyed polymer in chloroform solution at 5mg/ml was rotovapped at 600mbar and 60 °C in a 15x45mm with polyvinyl-faced pulp lined closure (Fisher) to form a uniform thin film. Solvent was monitored to prevent bumping and pressure was decreased stepwise from 800mbar at times. After total solvent removal, sample was placed under continuous vacuum overnight. The polymer was hydrated with desired pH solution for a concentration of 1mg/ml-2.5mg/ml at 60 °C and 200 RPM for 1 hour. Solution was then

sonicated for 20min at 100% power and 25kHz with ultrasonic bath sonicator (Elmasonic TI-H, Germany). Solution was passed through a 13mm 0.2um supor filter (Pall Corporation). Size characterization was carried using dynamic light scatter (DLS) on a Malvern Zetasizer NanoZS (Worcestershire, UK) and pH titration were conducted with the previously mentioned pH meter. Each titration point was allowed to equilibrate for 30min at 100 RPM.

Thin film hydration of 1.7kDa PEO-PAA vesicles at pH1 and DI H20, pH6.2 is displayed in Figure S11 before filtration. pH1 polymersomes read at ~220nm and changed only by 6-10nm during basic titration as shown in Figure S12. However the count rates, decrease substantially at every titration point indicating a loss of nano-species. Nano-structures formed at pH6.2 exhibit a large swelling from ~130nm and a PDI of 0.17 to ~640nm at pH1 with almost an unchanged PDI at 0.18, Figure S13. The response of the nanostructures, in either species loss or large swelling reflects that responses seen in the large gel re-hydrated structures

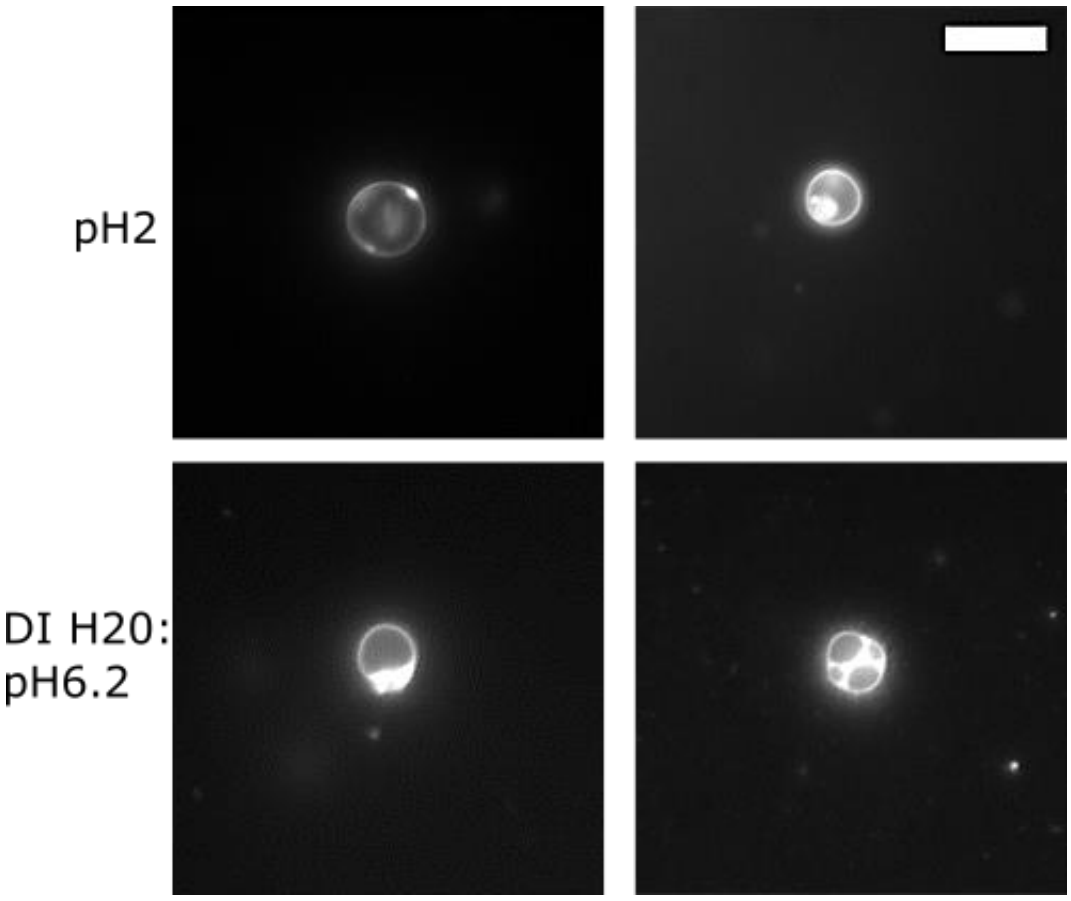

Figure S11. Thin film rehydration of acidic and neutral PEO-PAA 1.7kDa before filtration. Images were taken at 100x with scale bar set at 10μm.

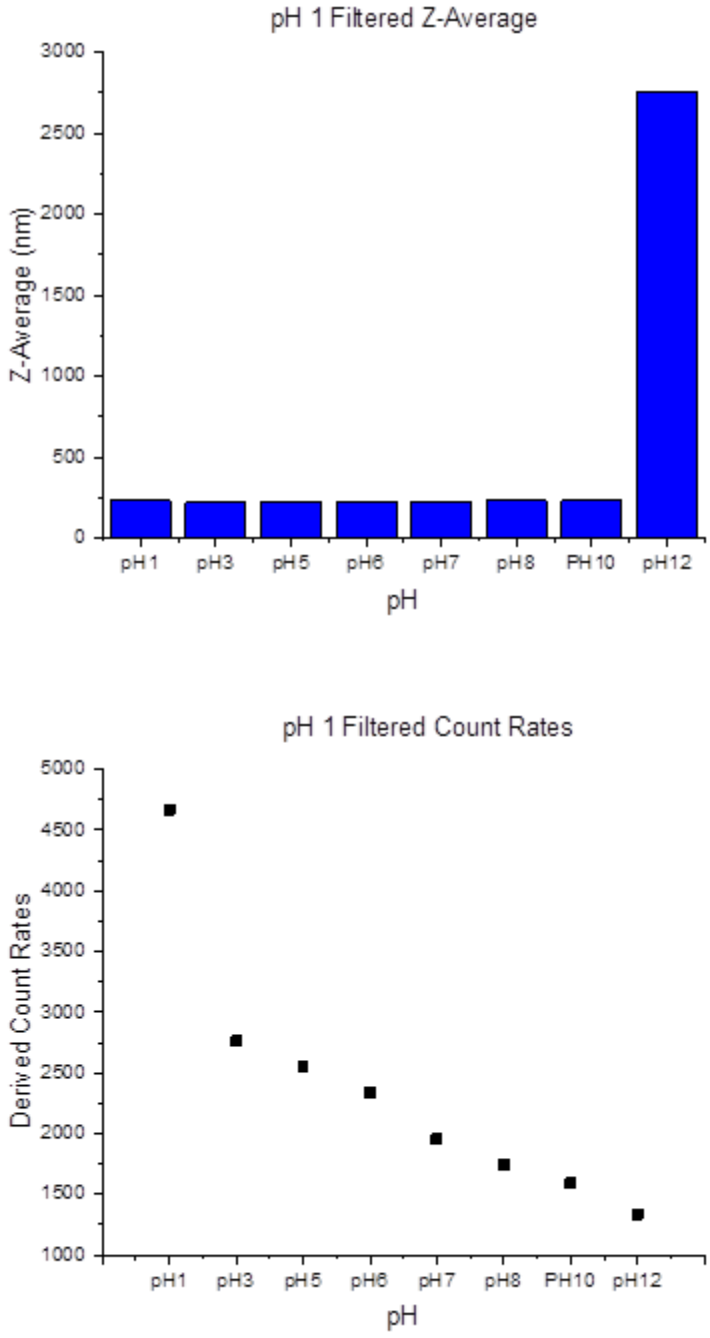

Figure S12. Titration of thin film formed acidic 1.7kDa PEO-PAA. Decrease in count rates indicate a loss of species. Polymersomes read at ~220nm and changed only by 6-10nm during basic titration

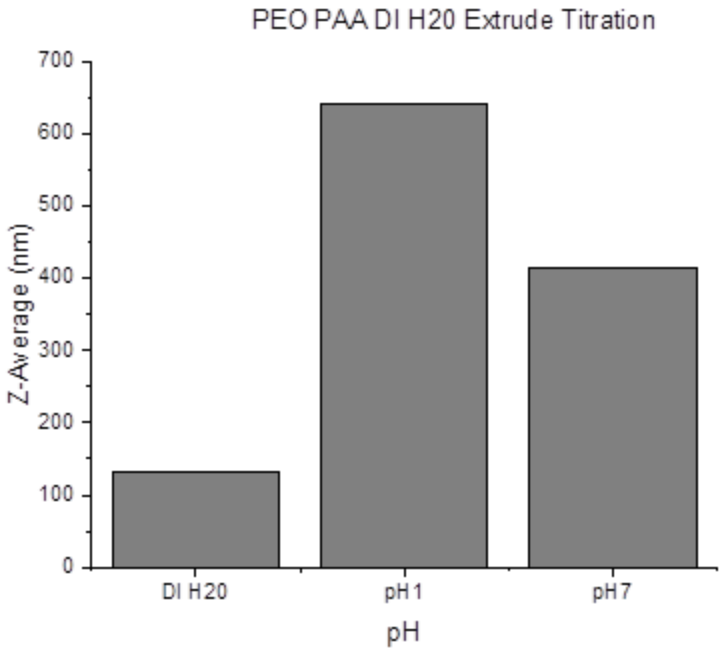

Figure S13. Acidic titration of neutral PEO-PAA 1.7kDa nanostructures formed by thin film hydration. PDI remains virtually unchanged from DIH20 to pH1 from 0.17 to 0.18. Titrating back up to pH7 yielded a PDI of 0.3.

References

[1] J. Schindelin, I. Arganda-Carreras, E. Frise, V. Kaynig, M. Longair, T. Pietzsch, S. Preibisch, C. Rueden, S. Saalfeld, B. Schmid, et al., *Nat. Methods* **2012**, *9*, 676–82.

[2] J. Liao, C. Wang, Y. Wang, F. Luo, Z. Qian, *Curr. Pharm. Des.* **2015**, *8324*.

CHAPTER 3

Polymeric Encapsulation of Mesoporous Silica Particles: The Future of Protocell Technology

Preface

Polymeric Encapsulation of Mesoporous Silica Particles: The Future of Protocell Technology highlights the capabilities of creating mesoporous silica particles encapsulated by responsive polymers. Giant polymer vesicle creation and synthesis of a unique dual-hydrophilic pH responsive diblock polymer were fundamental steps in improving the protocell technology-cargo loaded supported-lipid bilayer mesoprous silica particles. Replacing lipid bilayers with polymer systems, both distinctly synthesized and commercially available, allows for targeted release to virtually any biological stimuli.

Introduction

Protocells, mesoporous silica nanoparticles particles coated with supported lipid bilayers, have been shown to release multiple different drug cargos in endocytic conditions[1]. The mesoporous silica nanoparticle (MSNs) core can be loaded with a variety of drugs making it versatile not only for combinatorial cancer treatments[1–3],but for a variety of diseases and targeted gene therapy. Unlike traditional passive treatments of unbound drug that can exhibit limited selectivity and induce cell toxicity[1,4,5], nanocarrier systems, like the protocell, offer increased drug efficacy through enhanced targeting specificity.

Although this emerging technology is revolutionizing targeted delivery, use of supported lipid bilayers has inherent limitations. Unilamellar liposomes are constricted to

a bilayer thickness of 3 to 5 nm where polymersome bilayer thickness ranges from 8 to 21nm affording higher mechanical stability and a level of controlled release mechanics. Additionally, the chemical versatility through both functionality and block composition leads to limitless tunability of "smart" polymeric carriers that can respond to pH, ions, temperature, ultrasound, magnetization, or light[6–8]. Polymeric nanocarriers are an improvement to nanotherapeutic delivery systems, however the type of loaded cargo is largely dependent on polymer block formulation and is generally limited to a single species[8,9]. MSNs have been demonstrated to have good biocompatibility[10–14] and the high surface area of MSNs and tunable pore size allows for a range of cargo diversification, as well as promotes and the dissolution of the silica core network into nontoxic species[15].

Coupling "smart" polymers with MSNs will be the next generation of composite "sense-and respond" delivery systems and has gained traction over the past few years[16–26]. Polymer-MSN coupling has been shown with single polymers such as poly(ethylene glycol) (PEG or PEO)[24], poly(ethyleneimine) (PEI)[17] or pH sensitive polymers[20,23,26]. Copolymer construction onto the MSNs[18,25], MSN-copolymer electrostatic coupling[16], and multilayer polyelectrolyte-MSN constructs[19,22] have also been demonstrated with stimuli-responsive release. This has been vastly dependent on solution formed MSNs, and single type polymer or copolymer system that sometimes lack PEO.

Here we offer tailorable methods to improve targeted delivery by coupling evaporated induced self-assembly (EISA) MSNs with multiple responsive and multiple preformed polymer assemblies in lieu of lipids. Various diblock polymers that form not only polymersomes but also micelles can be coupled to multi-cargo loaded silica particles

to form a soft-matter hybrid delivery system. We demonstrate preliminary results of successful polymer-silica coating of diblock copolymers dominated by poly(ethylene oxide) (PEO, PEG), renowned for its biocompatibility and "stealth" [16,27–29] properties and pH responsive poly(acrylic acid) (PAA)[28,30–32] for both gastro intestinal targeted delivery and endocytic release.

Results and Discussion

Mesoporous silica particles , both nano and micron sized, were synthesized courtesy of Patrick Fleig of the Advanced Materials Laboratory using evaporation induced self-assembly (EISA)[33,34]. Modifications to the precursor sols and the EISA process were introduced in order to produce the desired pore and particle sizes. Nano-sized particles were produced using a TSI 3076 collision-type atomizer and nitrogen as the atomizing and carrier gas. Particles with 2 nm pores were produced from precursor solutions using cetrimonium bromide (CTAB) as the pore template (TEOS:EtOH:H20:HCl:CTAB 1:227:251:0.07:0.22 molar ratio). Particles with 6 nm pores were produced from precursor solutions containing Pluronic-F127 as the pore template (TEOS:EtOH:H20:HCl:F127 1:286:62:0.07:0.0064 molar ratio). Micron-sized particles were produced using a Sonotec 120kHz ultrasonic nebulizer. Particles with 2 nm pores were produced from precursor solutions using cetrimonium bromide (CTAB) as the pore template (TEOS:EtOH:H20:HCl:CTAB 1:286:62:0.07:0.22 molar ratio). Particles with 6 nm pores were produced from precursor solutions containing Pluronic-F127 as the pore template (TEOS:EtOH:H20:HCl:F127 1:286:62:0.07:0.0064 molar ratio). The templating agent was removed from the particles by calcination at 500 °C for 7 hours. Surface area and pore size were verified by nitrogen sorption (Micromeritics ASAP

2020) using BET[35] and BJH[36] analysis respectively. Particle size was verified using transmission electron microscopy (TEM, FEI Tecnai G2 S-Twin) image analysis (Figure 1) corresponding to ~97nm form nanoparticles and ~3-10μm for micron particles per TEM. Effort was taken to make micron sized particles because it provides the useful visualization of any polymeric coupling.

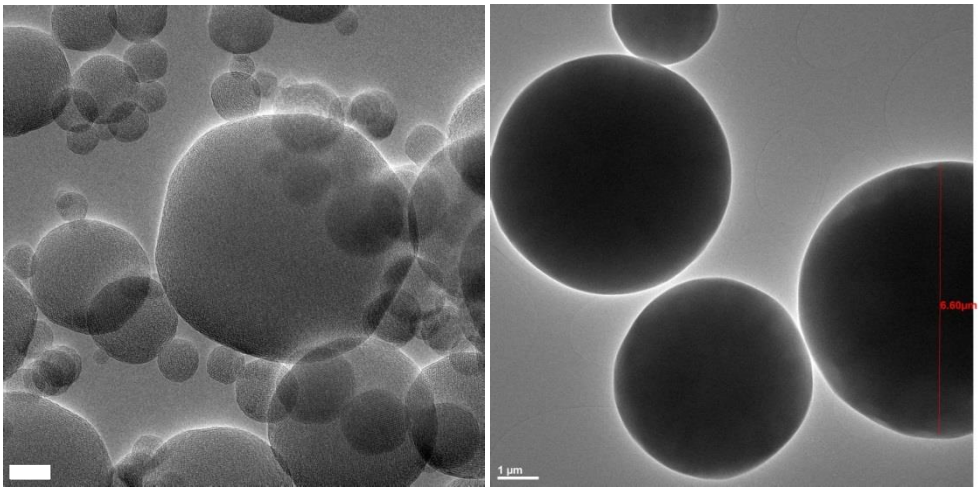

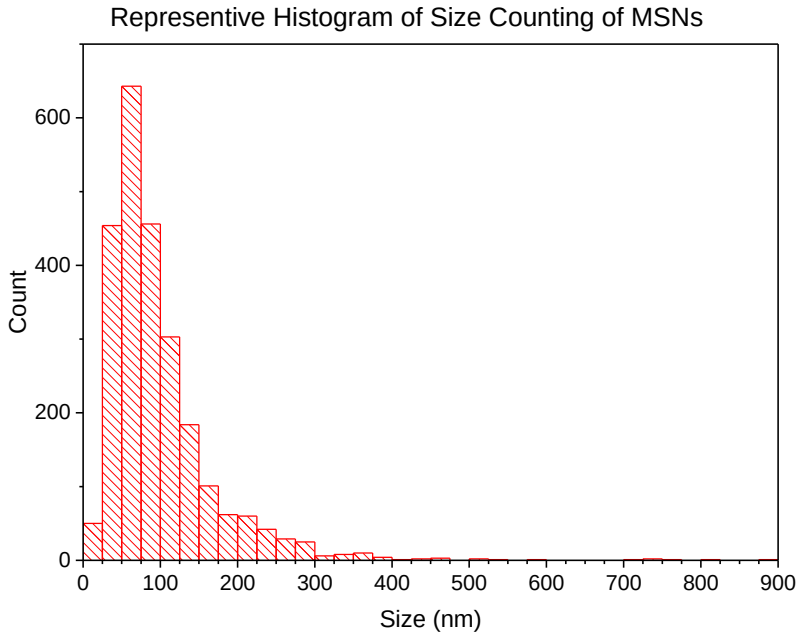

Figure 1. TOP: Left image is representative of CTAB pore template nanoparticles with a scale bar at 50nm. Right image is representative of both CTAB and F127 pore template micron particles ranging from ~3-10µm.
BOTTOM: Manual TEM grid counting of represented EISA nanoparticle batch was done in collaboration with Gabriel Garcia, Patrick Fleig, and Brandon Slaughter with an n=3 and over 2000 events measured for each. Typical particle size per TEM was ~97nm and standard deviation of 73.5nm.

Effective Post Silanization Modification of Silica Particles

Characterization of the nanoparticles was also conducted by dynamic light scattering DLS (Malvern Zetasizer NanoZS) generally at 0.1mg/ml. However, as seen in the histogram, some large particles are produced which greatly skew the intensity profile of DLS. Typical Z-average in DIH20 ranges from ~300-320nm with a poly dispersity index (PDI) typically at 0.17-0.20 and EtOH ranges from ~400-420nm with a PDI from 0.20-0.30 (data not shown). It is noted that number DLS is a measure of solvent shell around the particle and not of the dry core as in TEM so differences are expected.

In an attempt to size excluded larger MSN species, dead-end filtration was utilized. Not surprisingly, it was discovered that most of the particles were captured in the PES filter membrane due to membrane particle interaction. Some success was found in using surfactant free cellulose acetate membranes (SFCA) that typically lowered the size by ~100nm according to DLS, but yields were low. It is noted that un-calcined particles may be more appropriate for dead-filtration as membrane interactions may be minimized. For these initial studies, separation was not needed, but for a smaller population range centrifugation for 4.5min at 500 rcf was used to remove a population of larger particles and produced a sufficient DLS Z-average size of 270.1nm at PDI 0.145 (Figure 2).

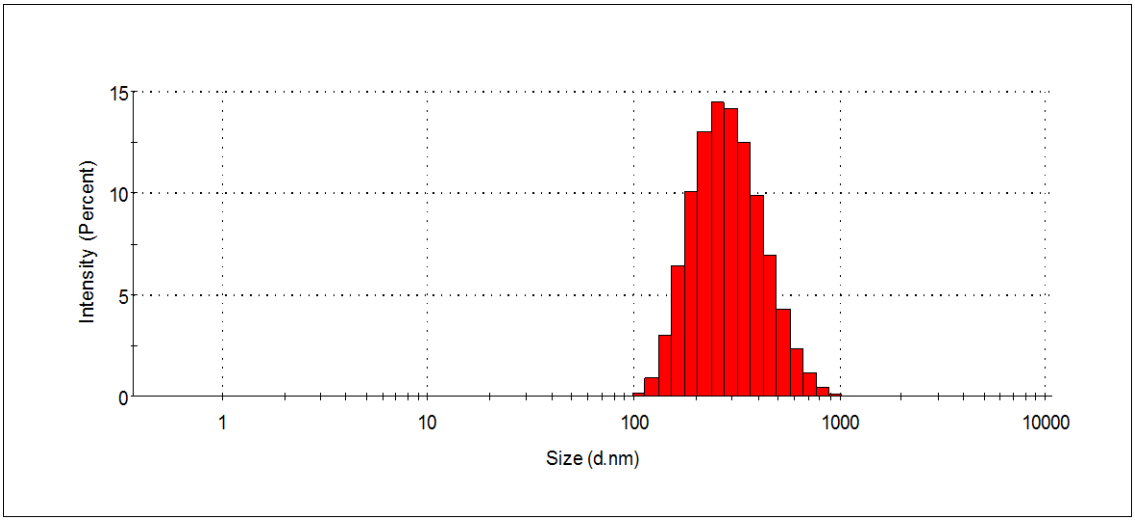

Figure 2. DLS of MSNs after centrifugation at 4.5min and 500rcf. Z-average of 270.1nm and PDI of 0.145

Post-silanization processes is an effective method that allows altering the silica surface chemistry for bio-coupling and multiple different functionalities through alkoxysilanes[15]. Silanization of MSNs was carried out by mixing interchangeable volume percent of aminosilanes in 95%EtOH and DIH20 (DIH20 was kept at 5vol% and vol% of 95%EtOH was adjusted dependent on aminosilane vol%). The alkoxysilanes was allowed to hydrolyze for 5 minutes before adding to 2mg of MSNs at a concentration of 2mg/ml. The solution was sonicated for 1hr at 25kHz and 100% power in an ultrasonic bath sonicator. (Elmasonic TI-H, Germany). The particles were concentrated at 20,000rcf form 15 min and washed in MeOH 3x. The functionalized particles were then dried overnight under vacuum. Functionalized MSNS were re-suspended in DIH20 and characterized by DLS at 0.1mg/ml. The alkoxysilanes studied were (3-Aminopropyl)triethoxysilane (APTES,Gelest), and N-(6-aminohexyl)aminomethyltriethoxysilane (AHAMTES: Gelest). 3.7kDA PEG silane(Nanocs) and Methoxy(polyethyleneoxy)propyl trimethoxysilane (GELEST) was

attempted, but results were inconsistent under these conditions. APTES was chosen as it is a common silane used for coupling molecules[37]. AHAMTES was utilized per claims that it provides better particle colloidal stability over shorter chain aminosilanes[38]. Post-MSNs synthesis surface silanization generally always produced aggregation as seen in Table 2 and 3. Aggregation was an indication that surface modification occurred but additional verification was conducted by zeta potential measurements, if aggregation was not present (compared to zeta potential of unmodified MSNs -30.5mV (Table 1) with a typical range from -30 to -40mV). Aggregation is not desired in any future nanoparticle biomedical application and one mitigation process is introducing alkoxysilanes into the precursor solution[1]. This can produce MSNs with a functional surface, but calcination is no longer an option as the high temperatures are damaging to the alkoxysilanes and solvent surfactant extraction (typically in EtOH) must be used. Furthermore, in-house experiments have shown that different pore template surfactants have a certain resistance to common solvent extraction techniques. Acidifying the amino silanized MSNs, created post-particle synthesis, resulted in the breaking apart of aggregates as seen in the DLS of 240nm and still maintained a level of surface functionality at all silane concentrations expressed by the +40mV to +50mVzeta potential seen in Table 4. Amino functionalized MSNs were spun at 20,000 rcf and 15min and transferred into a HCl (Fisher) pH1 solution. The particles were allowed to incubate for 40 min and where cleaned 1-2x at the same spin rate and speed before characterization by DLS. Particles were then cleaned 2-3x in DIH20 (~ph4.0) and resulted in improved DLS 238.8nm and Zeta 39.2mV for APTES MSNS. The results for the AHAPS resuspension in DIH20 were inconclusive given that the zeta was very close to that of regular unmodified MSNS.

Table 1.

MSNs in DIH20	
Z-Average (nm)	325.6
PDI	0.195
Zeta (mV)	-30.5

Table 2.

APTES	2%	1%	0.0625%
Z-Average (nm)	1347	Sedimentation	452.1
PDI	0.442	-	0.423
Zeta (mV)	-	-	9.67

Table 3.

AHAPTES	2%	1%	0.0625%
Z-Average (nm)	1567	445.3	256.5
PDI	0.378	0.341	0.232
Zeta (mV)		-16.16	-20.53

Table 1: Top Control of MSN cores.**Table 2: Middle** APTES silanization, **Tab 3: Bottom** AHAPTES silanization. Silanization was conducted at various volume percent read in DIH20. Zeta potential was not read if large aggregates were present. There is a clear decrease in size trend with decreasing silane. Control sample of MSN cores is displayed on the top.

Table 4.

Surface	Z-average(nm)	PDI	Zeta (mV)
MSN Cores	281.2	0.159	2.92
APTES	246.7	0.154	53.6
AHAPTES	245.3	0.151	43

Table 4: Acidification of 2vol% silanized MSNS. Same trend was seen in lower concentrations of silane.

The mechanism that describes the silanization process is shown in Schematic 1 adapted from Liu et al.[39] Most likely the amino silanization is causing particle interaction by H-bonding, or forming multi-layers. Acidification provides charge stability to prevent hydrogen bonding, ionic interaction and possibly breaks apart multi-layer silanes. It is noted that this could also potentially break apart siloxane bonds.

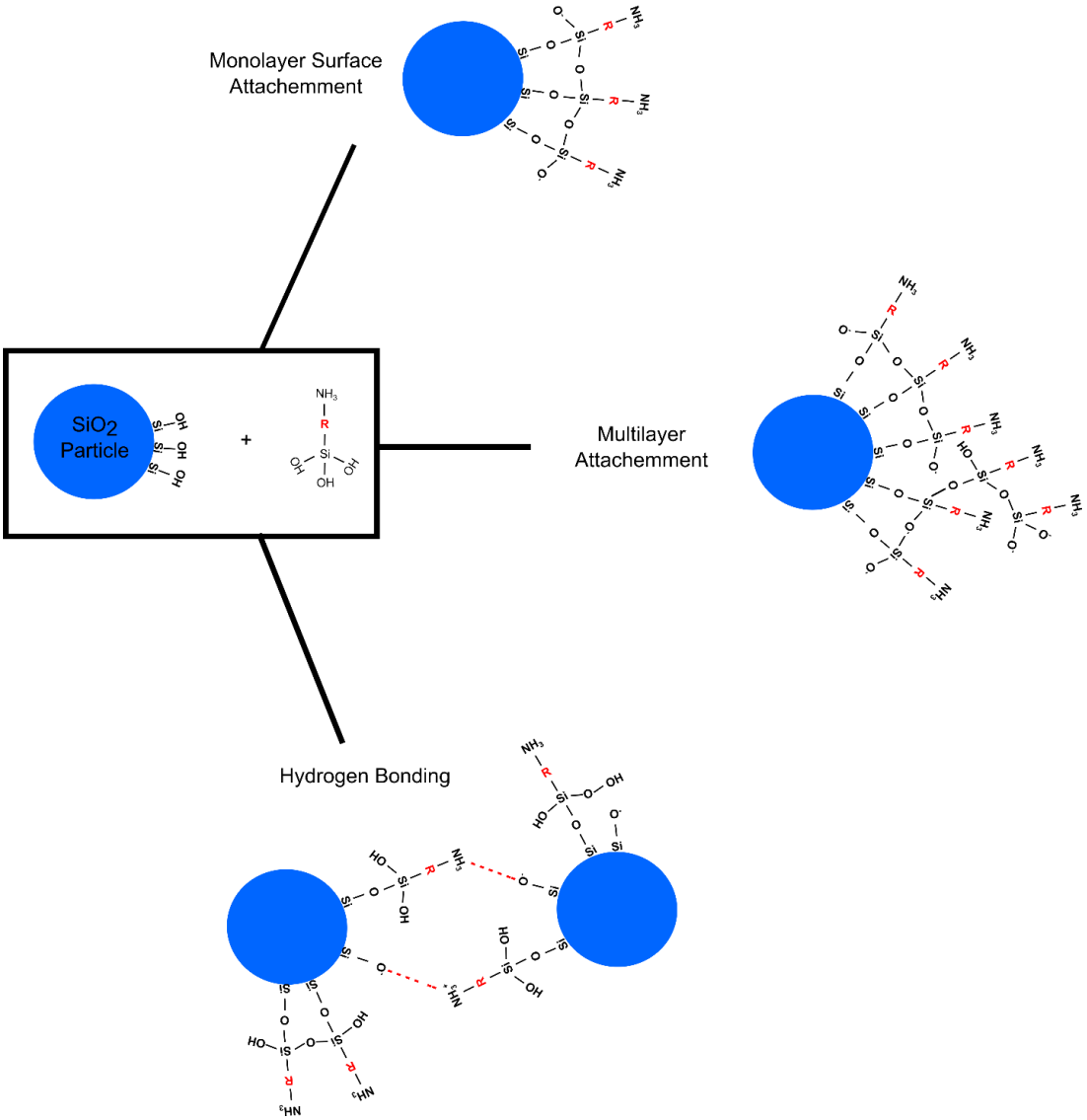

Schematic 1. 3 reaction methods of amino silanization of MSNs adapted from Liu et al[39].

Preliminary Coupling of Polymersomes and Polymeric Micelles to Mesoporous Particles

Surface functionalization of synthesized MSNs is an integral step in producing customizable delivery system. The next progression of the polymeric protocell system is to prove successful self-assembly polymersome or micelle coating. We propose using the following diblocks and diblock blends with corresponding molecular structures (Figure 3).

1. Poly(butadiene)-b-poly(ethylene oxide) (PBD-PEO)
2. Carboxylic Acid functionalized Poly(butadiene)-b-poly(ethylene oxide) (PBD-PEO-COOH)
3. Amine functionalized Poly(butadiene)-b-poly(ethylene oxide) (PBD-PEO-NH^{2+})
4. Poly(butadiene)-b-poly(acrylic acid) (PBD-PAA)
5. Poly(styrene)-b-poly(acrylic acid) (PS-PAA)
6. Poly(ethylene oxide)-b-poly(acrylic acid) (PEO-PAA)
7. PEO-PAA:PBD-PAA blend
8. PEO-PBD:PBD-PAA blend

Options 1 through 5 have distinct hydrophilic blocks (PEO or PAA) and hydrophobic blocks (PBD or PS). Option 6 is the unique self-assembly dual-hydrophilic polymer as described in Chapter 2. Functionalized polymers, option 2 and 3 represent another level of customization to nano-delivery systems. Lastly, option 7 and 8 represent potentially useful polymer blends. Rational for using PEO and PAA as previously discussed is due to the stealth characteristics of PEO and pH responsiveness to PAA. PS

was chosen because it has been demonstrated to absorb into the endothelial lining within the gastro intestinal tract[40].

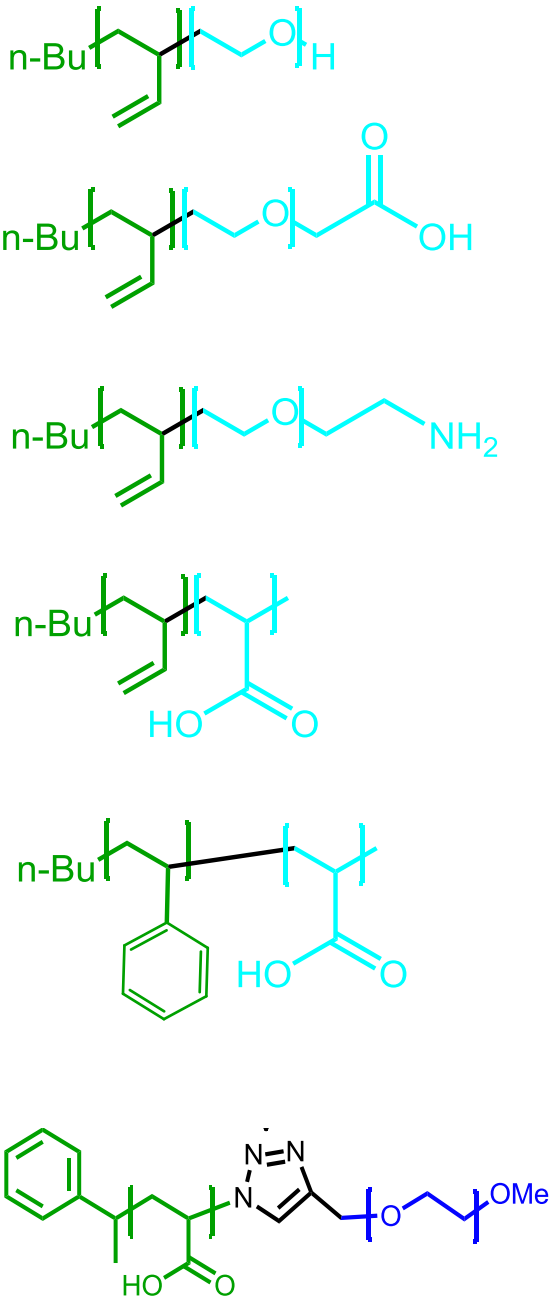

1. PBD-PEO
2. PBD-PEO-COOH
3. PBD-PEO-NH^{2+}
4. PBD-PAA
5. PS-PAA
6. PEO-PAA

Figure 3. Chemical structures of proposed self-assembly diblock polymers to couple with mesoporous silica particle. Option 7 PEO-PAA:PBD-PAA blend is a combination of diblock 6 and diblock 4. Option 8 PEO-PBD:PBD-PAA is a combination of diblock 1 and diblock 4.

Currently, PEO-PBD (PBD_{2000}-PEO_{950}, Polymer Source), PEO-PBD-COOH, PEO-PBD-NH2, PBD-PAA (PBD_{1000}-PAA_{2200}, Polymer Source), and PEO-PAA (synthesized by Ian Henderson per Chapter 2), have been self-assembled by film hydration as described in Chapter 2. All polymers were hydrated at a 2.5mg/mL concentration with 0.5 mol% of either Lissamine Rhodamine B PE lipid or 0.5 mol% NBD-PC lipid (Avanti Polar Lipids, Inc., Alabaster, AL). Polymersomes were either extruded or filtered through poly carbonate membranes (PC,Whatman) or Supor polyether sulfone membranes (PES, Pall Corporation) dependent on pH of hydration solvent. Rehydration parameters and DLS size are shown in Table 5. Polymersomes and polymeric micelles were incubated with micron porous silica particles with pores templated by either F127 or CTAB from 1-4 hours and resulted in successful coating (Figure 4). Only PEO-PBD-NH2 polymersome have been attempted to coat MSNs which was verified by both in TEM (data not shown) and change in zeta potential from -37.5mV for bare MSNs to +45.1mV for PEO-PBD-NH2 coated MSNs.

Polymer	**M_w(total)**	**Rehydration pH**	**Membrane**	**DLS (nm)**
PEO-PBD-NH^{2+}	2950	pH6.2, DIH20	0.45μm 19mm PC Extruded	415.7
PEO-PBD-COO^-	2950	pH6.2, DIH20	0.4μm 19mm PC Extruded	438.9nm
PEO-PAA	3050	pH1	0.45μm 13mm PES Filtered	141.9
PBD-PAA (micelle)	3200	pH1		37.64

Table 5. Film hydration parameters and corresponding DLS before coating

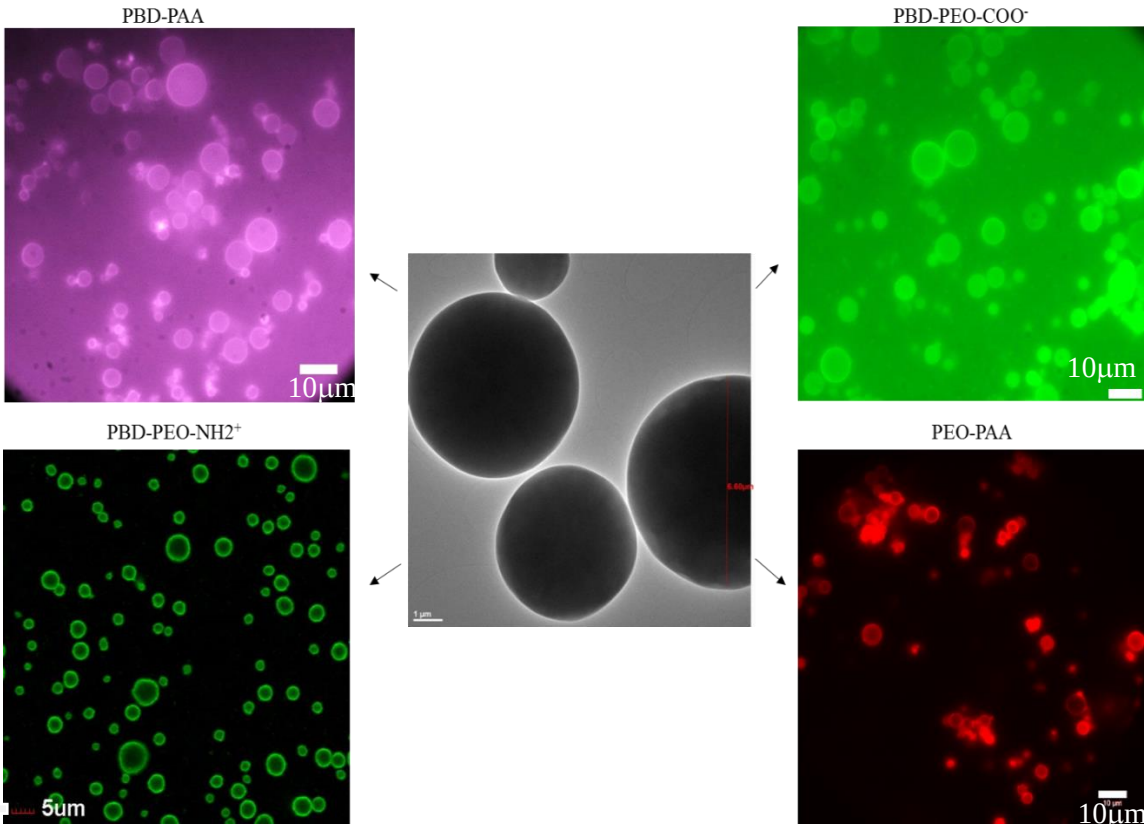

Figure 4. Self-assembly polymer structures coupled to mesoporous micron silica particle (middle image taken by TEM) making a soft-matter composite material (surrounding images). Scale bars are shown on each image.

Future Work

Currently, we have promising results of a post-synthesis silanization on EISA MSNs that reverses aggregation and provides cationic functionalization of the silica cores. Furthermore, 4 of the 8 proposed diblock copolymers have been shown to effectively coat the mesoporous silica particles. Future experiments to complete this promising study would be to investigate the complete array of diblock copolymers coupling to nanoparticles and micron particles, independent investigation of polymersome/micelle reaction to pH changes, and pH triggered release of drug loaded polymer-MSNs complexes through both alkalization and acidification using the proposed

copolymers. The ability to couple multiple different diblock copolymers allows for modularity and the ability to make the protocell system tailorable for any therapeutic treatment.

References

[1] C. E. Ashley, E. C. Carnes, G. K. Phillips, D. Padilla, P. N. Durfee, P. a Brown, T. N. Hanna, J. Liu, B. Phillips, M. B. Carter, et al., *Nat. Mater.* **2011**, *10*, 389–397.

[2] C. E. Ashley, E. C. Carnes, K. E. Epler, D. P. Padilla, G. K. Phillips, R. E. Castillo, D. C. Wilkinson, B. S. Wilkinson, C. a Burgard, R. M. Kalinich, et al., *ACS Nano* **2012**, *6*, 2174–2188.

[3] K. Epler, D. Padilla, G. Phillips, P. Crowder, R. Castillo, D. Wilkinson, B. Wilkinson, C. Burgard, R. Kalinich, J. Townson, et al., *Adv. Healthc. Mater.* **2012**, *1*, 348–353.

[4] D. Peer, J. M. Karp, S. Hong, O. C. Farokhzad, R. Margalit, R. Langer, *Nat. Nanotechnol.* **2007**, *2*, 751–760.

[5] M. Ferrari, *Nat. Rev. Cancer* **2005**, *5*, 161–171.

[6] D. E. Discher, F. Ahmed, *Annu. Rev. Biomed. Eng.* **2006**, *8*, 323–341.

[7] F. Meng, Z. Zhong, J. Feijen, *Biomacromolecules* **2009**, *10*, 197–209.

[8] W. Chen, F. Meng, R. Cheng, Z. Zhong, *J. Control. Release* **2010**, *142*, 40–46.

[9] H. Cabral, K. Kataoka, *J. Control. Release* **2014**, *190*, 465–476.

[10] F. Tang, L. Li, D. Chen, *Adv. Mater.* **2012**, *24*, 1504–1534.

[11] Y. Wang, Q. Zhao, Y. Hu, L. Sun, L. Bai, T. Jiang, S. Wang, *Int. J. Nanomedicine* **2013**, *8*, 4015–4031.

[12] M. Kilpeläinen, J. Riikonen, M. a. Vlasova, a. Huotari, V. P. Lehto, J. Salonen, K. H. Herzig, K. Järvinen, *J. Control. Release* **2009**, *137*, 166–170.

[13] J. Lu, M. Liong, Z. Li, J. I. Zink, F. Tamanoi, *Small* **2010**, *6*, 1794–1805.

[14] X. Huang, L. Li, T. Liu, N. Hao, H. Liu, D. Chen, F. Tang, *ACS Nano* **2011**, *5*, 5390–5399.

[15] D. Tarn, C. E. Ashley, M. Xue, E. C. Carnes, J. I. Zink, C. J. Brinker, *Acc. Chem. Res.* **2013**, *46*, 792–801.

[16] G.-F. Luo, W.-H. Chen, Y. Liu, Q. Lei, R.-X. Zhuo, X.-Z. Zhang, *Sci. Rep.* **2014**, *4*, 1–10.

[17] T. Xia, M. Kovochich, M. Liong, H. Meng, S. Kabehie, S. George, J. I. Zink, A. E. Nel, *ACS Nano* **2009**, *3*, 3273–3286.

[18] H. Meng, M. Xue, T. Xia, Z. Ji, D. Y. Tarn, J. I. Zink, A. E. Nel, *ACS Nano* **2011**, *5*, 4131–4144.

[19] Y. Sun, Y. L. Sun, L. Wang, J. Ma, Y. W. Yang, H. Gao, *Microporous Mesoporous Mater.* **2014**, *185*, 245–253.

[20] J. T. Sun, C. Y. Hong, C. Y. Pan, *J. Phys. Chem. C* **2010**, *114*, 12481–12486.

[21] H. Tang, J. Guo, Y. Sun, B. Chang, Q. Ren, W. Yang, *Int. J. Pharm.* **2011**, *421*, 388–396.

[22] J. Wang, H. Liu, F. Leng, L. Zheng, J. Yang, W. Wang, C. Z. Huang, *Microporous Mesoporous Mater.* **2014**, *186*, 187–193.

[23] K.-N. Yang, C.-Q. Zhang, W. Wang, P. C. Wang, J.-P. Zhou, X.-J. Liang, *Cancer Biol. Med.* **2014**, *11*, 34–43.

[24] S. Bhattacharyya, H. Wang, P. Ducheyne, *Acta Biomater.* **2012**, *8*, 3429–3435.

[25] B. Chang, D. Chen, Y. Wang, Y. Chen, Y. Jiao, X. Sha, W. Yang, *Chem. Mater.* **2013**, *25*, 574–585.

[26] H. Peng, R. Dong, S. Wang, Z. Zhang, M. Luo, C. Bai, Q. Zhao, J. Li, L. Chen, H. Xiong, *Int. J. Pharm.* **2013**, *446*, 153–159.

[27] R. P. Brinkhuis, F. P. J. T. Rutjes, J. C. M. van Hest, *Polym. Chem.* **2011**, *2*, 1449.

[28] Q. Liu, J. Chen, J. Du, *Biomacromolecules* **2014**, *15*, 3072–3082.

[29] J. S. Lee, K. D. Park, **2011**, *15*, 152–158.

[30] V. V Khutoryanskiy, A. V Dubolazov, Z. S. Nurkeeva, G. a Mun, *Langmuir* **2004**, *20*, 3785–3790.

[31] a. K. Bajpai, S. K. Shukla, S. Bhanu, S. Kankane, *Prog. Polym. Sci.* **2008**, *33*, 1088–1118.

[32] S. Ganta, H. Devalapally, A. Shahiwala, M. Amiji, *J. Control. Release* **2008**, *126*, 187–204.

[33] Y. Lu, H. Fan, a. Stump, T. L. Ward, T. Rieker, C. J. Brinker, *Nature* **1999**, *398*, 223–226.

[34] C. J. Brinker, Y. Lu, A. Sellinger, H. Fan, *Adv. Mater.* **1999**, *11*, 579–585.

[35] S. Brunauer, P. H. Emmett, E. Teller, *J. Am. Chem. Soc.* **1938**, *60*, 309–319.

[36] E. P. Barrett, L. G. Joyner, P. P. Halenda, *J. Am. Chem. Soc.* **1951**, *73*, 373–380.

[37] E. A. Smith, W. Chen, *Langmuir* **2008**, *24*, 12405–12409.

[38] C. Graf, Q. Gao, I. Schütz, C. N. Noufele, W. Ruan, U. Posselt, E. Korotianskiy, D. Nordmeyer, F. Rancan, S. Hadam, et al., *Langmuir* **2012**, *28*, 7598–7613.

[39] Y. Liu, Y. Li, X. Li, T. He, *Langmuir* **2013**, *29*, 15275–15282.

[40] S. H. Bakhru, S. Furtado, a. P. Morello, E. Mathiowitz, *Adv. Drug Deliv. Rev.* **2013**, *65*, 811–821.